Orco regulates the circadian activity of pheromone-sensitive olfactory receptor neurons in hawkmoths

Abbreviated title: Circadian regulation by Orco

Author names and affiliations:
* Aditi Vijayan, Animal Physiology and Center for Interdisciplinary Nanostructure Science and Technology, FB 10, University of Kassel, 34132 Kassel, Germany
* Mauro Forlino, Theoretical Physics and Center for Interdisciplinary Nanostructure Science and Technology, FB10, University of Kassel, 34132 Kassel, Germany
Yajun Chang, Animal Physiology and Center for Interdisciplinary Nanostructure Science and Technology, FB 10, University of Kassel, 34132 Kassel, Germany
Pablo Rojas, Theoretical Physics and Center for Interdisciplinary Nanostructure Science and Technology, FB10, University of Kassel, 34132 Kassel, Germany
Katrin Schröder, Animal Physiology and Center for Interdisciplinary Nanostructure Science and Technology, FB 10, University of Kassel, 34132 Kassel, Germany
Anna C. Schneider, Animal Physiology and Center for Interdisciplinary Nanostructure Science and Technology, FB 10, University of Kassel, 34132 Kassel, Germany
Martin E. Garcia, Theoretical Physics and Center for Interdisciplinary Nanostructure Science and Technology, FB10, University of Kassel, 34132 Kassel, Germany
Monika Stengl, Animal Physiology and Center for Interdisciplinary Nanostructure Science and Technology, FB 10, University of Kassel, 34132 Kassel, Germany
*Both authors contributed equally
Corresponding author email address: anna.c.schneider@uni-kassel.de

Conflict of interest: Authors report no conflict of interests.
Acknowledgements: We thank Dr. Dieter Wicher (Max Planck Institute for Chemical Ecology, Jena, Germany) for generously providing OLC15, and Rishaban Radhakrishnan for help with Python codes. We thank Prof. Hülya Altuntaş for helpful discussions.
Funding: AV, MF, YC, ACS, MEG, and MS were supported by Deutsche Forschungsgemeinschaft RTG 2749/1: “Biological Clocks on Multiple Time Scales”; KS and MS were supported by Deutsche

Forschungsgemeinschaft STE531/20-2; PR was supported through the Add-on Fellowship for Interdisciplinary Life Science by the Joachim Herz Foundation.

Author contributions:

Conceptualization: AV, MF, MEG, MS; data curation: AV, MF, YC, PR, KS, ACS, MEG, MS; formal analysis: AV, MF, YC, PD, ACS; funding acquisition: MEG, MS; investigation: AV, MF, YC, KS; methodology: MF, PR, MEG, MS; project administration: ACS, MEG, MS; resources: MEG, MS; software: AV, MF, PR, MEG; supervision: MEG, MS; validation: AV, MF, YC, PR, KS, ACS, MEG, MS; visualization: AV, MF, YC, ACS, MS; writing – original draft: AV, MF, ACS, MEG, MS; writing – reviewing & editing: AV, MF, YC, ACS, MEG, MS.

1 Abstract

The mating behavior of nocturnal *Manduca sexta* hawkmoths is under strict temporal control. It is orchestrated via circadian and ultradian oscillations in sex-pheromone stimuli as social zeitgeber. The extremely sensitive pheromone-detecting olfactory receptor neurons (ORNs) that innervate the long trichoid sensilla on the male's antennae are peripheral circadian clocks. They express the transcriptional-translational feedback loop (TTFL) circadian clockwork, best characterized in *Drosophila melanogaster*. In hawkmoths, it is still unknown whether or how the ORN TTFL clockwork regulates the daily rhythms in pheromone sensitivity and in temporal resolution of ultradian pheromone pulses as prerequisites to the temporal regulation of hawkmoth mating behavior.

We hypothesize that, rather than the slow TTFL clock, a more rapidly adaptive post-translational feedback loop (PTFL) clockwork, associated with the ORN plasma membrane, allows for temporal control of pheromone detection via generation of multiscale endogenous membrane potential oscillations. The potential oscillations of the PTFL clock could rapidly synchronize to oscillations of pheromone stimuli at different timescales, thus enabling the prediction of stimulus patterns as a mechanism for active sensing. With *in vivo* long-term tip recordings of long trichoid sensilla of male hawkmoths, we analyzed the spontaneous spiking activity indicative of the ORNs' endogenous membrane potential oscillations. Consistent with our hypothesis of a multiscale PTFL clock in hawkmoth ORNs, spontaneous spiking was modulated on ultradian and circadian timescales, with maximum activity at night. When we blocked the evolutionarily conserved olfactory receptor coreceptor (Orco), the circadian modulation was abolished but the ultradian frequency modulation of the spontaneous activity remained. Consistent with PTFL control, Orco was not under the transcriptional control of the TTFL clock, but its modulation was dependent on cAMP. We could replicate the experimental data in a conductance-based computational model of an ORN. In this model, Orco conductivity changed as a function of fluctuating 2nd messenger levels. This study demonstrates that a PTFL clock is sufficient to impose a circadian pattern on ORN sensitivity.

2 Significance statement

It is generally assumed that all circadian rhythms in an organism are driven by a transcriptional-translational feedback loop (TTFL) clock. In this study, we demonstrate with *in vivo*

recordings of hawkmoth pheromone-sensitive olfactory receptor neurons (ORNs) that the olfactory receptor coreceptor (Orco) is the key pacemaker channel for controlling circadian, but not all ultradian, rhythms in spontaneous spiking activity. Since Orco expression is not driven by the TTFL clock, its conductance appears to be controlled by a post-translational feedback loop (PTFL) membrane clock via 2nd messengers. Accordingly, our computational model suggests that ORN sensitivity is tuned by periodic changes in the conductivity of an Orco ion channel, which is mediated by cycling levels of cyclic nucleotides. This highlights the role of the contribution of posttranslational modifications to the generation of circadian rhythmicity.

3 Introduction

Biological clocks generate endogenous physiological and behavioral oscillations on multiple timescales that persist in the absence of any external timing cues under constant conditions (Lamont and Amir, 2010). Such clocks are essential to generate internal rhythms and to permit their synchronization to external zeitgebers at timescales from milliseconds to years. These synchronized endogenous multiscale clocks thus provide both a continuous time frame for physiology and behavior - the organism's "present time" - and enable organisms to predict and respond to regular, periodic environmental changes (Stengl and Schneider, 2024). Even though endogenous clocks are widespread in prokaryotes and eukaryotes (Géron et al., 2024; Hall and Rosbash, 1993; Millar, 2016; Thaiss et al., 2014), current knowledge about how multiscale clocks are linked over widely diverging timescales remains sparse.

Insect circadian clock neurons, which are tightly connected to visual brain circuits, are amongst the best studied biological clocks (Hall and Rosbash, 1993; Nishiitsutsuji-Uwo and Pittendrigh, 1968; Reinhard et al., 2024). They regulate physiological and behavioral oscillations that underly sleep-wake rhythms tied to the 24 h light-dark cycles on Earth (Dubowy and Sehgal, 2017). Circadian clock neurons possess a molecular clockwork of transcriptional-translational feedback loops (TTFLs). This TTFL clock generates endogenous oscillations of clock gene mRNA and protein levels with a cycle period of ~24 h via negative feedback by proteins that inhibit their own transcription (Hardin, 2011). It is assumed for both insects and mammals that this TTFL comprises the master clockwork that regulates all physiological and behavioral rhythms in the circadian time range through genetically controlled output pathways (Hastings et al., 2020).

Molecular TTFL clockworks were not only found in central brain clock neurons but also in sensory neurons, such as olfactory receptor neurons (ORNs) in insect antennae, where they play a role in odor-dependent circadian behaviors like feeding, pollination, reproduction, and navigation (Flecke et al., 2010; Flecke and Stengl, 2009; Krishnan et al., 1999; Merlin et al., 2009, 2006; Page and Koelling, 2003; Plautz et al., 1997; Sauman and Reppert, 1998; Schendzielorz et al., 2015; Schuckel et al., 2007; Tanoue et al., 2004; Zhou et al., 2005). Little is known about how the TTFL clockwork of insect ORNs regulates circadian rhythms in chemosensory sensitivity that underlie the circadian control of these different behaviors.

At night, male nocturnal *Manduca sexta* hawkmoths are very sensitive to the sex pheromone blend that their conspecific females release in an intermittent pattern (Itagaki and Conner, 1988). The intermittency is a prerequisite to maintain the male's search flight, which is suspended at pulse frequencies >30 Hz (Baker et al., 1985; Baker and Vogt, 1988; Stengl, 2010). The pheromone pulses are resolved of up to 3 Hz by pheromone-specific ORNs in the antenna's long trichoid sensilla (Lee and Strausfeld, 1990; Marion-Poll and Tobin, 1992). Pheromone-specificity is provided by odor receptor (OR) subunits in the ciliary membranes of ORNs that heteromerize with the conserved olfactory receptor co-receptor Orco (Nakagawa and Vosshall, 2009; Stengl and Funk, 2013; Wicher and Miazzi, 2021). The insect odor transduction cascade is still under debate and seems to involve both ionotropic and metabotropic pathways (Sato et al., 2008; Schneider et al., 2025; Wicher et al., 2008). While there is no general agreement on the role of Orco, it is known that in heterologous expression systems Orco homo- and heteromers form a slow, leaky, non-specific cation channel, which depolarizes the cells (Jones et al., 2011; Sargsyan et al., 2011; Sato et al., 2008; Wicher, 2018; Wicher et al., 2008). *In vivo* tip recordings of long trichoid sensilla in *M. sexta* confirmed that Orco acts as leaky cation channel, acting as a pacemaker channel, because it promotes ultradian membrane potential oscillations that underly the spontaneous action potential activity (Nolte et al., 2013). These potential oscillations turn the ORNs into ultradian temporal filters that are sensitive to the frequency of the pheromone pulses they encounter. Pheromone pulses that arrive at a similar frequency as the endogenous sub-threshold membrane potential oscillations would synchronize these oscillations and would be more likely to elicit action potential trains. Therefore, this pacemaker channel-dependent mechanism would allow for active sensing if endogenous membrane potential oscillations are in the physiological range that is necessary for tracking intermittent pheromone pulses.

131 It is not known whether the Orco-dependent membrane potential oscillations also occur at
132 circadian timescales, and whether or how they are linked to ultradian potential oscillations. One
133 hypothesis is that the molecular TTFL clockwork of ORNs exclusively controls endogenous
134 circadian rhythms of the membrane potential via circadian expression of pacemaker channels like
135 Orco. Alternatively, the plasma membrane of ORNs could by itself constitute an autonomous clock
136 that is entrained by but does not rely on the TTFL clock. Constant levels of ion channels that do not
137 require daily degradation and daily transcription via the TTFL clock, but with modulation of open-
138 time probability by posttranslational modifications, would constitute a more economical and
139 faster adjustable mechanism to generate endogenous membrane potential oscillations (Stengl and
140 Schneider, 2024). This would facilitate active sensing by rapidly tuning odorant/pheromone
141 detection to behaviorally relevant zeitgeber signals in the insect's environment.
142 Here, we performed a combination of experimental and computational modeling studies to
143 investigate whether Orco plays a role in active sensing at the circadian and/or ultradian timescale
144 via generation of endogenous membrane potential oscillations. We hypothesize that Orco is part of
145 a post-transcriptional feedback loop (PTFL) clockwork in the plasma membrane, rather than being
146 TTFL controlled. To capture naturally occurring, physiologically relevant processes in insect ORNs
147 we performed *in vivo* long-term tip recordings of the spontaneous spiking activity of pheromone-
148 sensitive trichoid sensilla of intact but restrained hawkmoth males.
149 We corroborated the experimental data with a Hodgkin-Huxley (HH) based computational
150 ORN model. In general, the widely used deterministic HH models do not include circadian control
151 of ion channels. Moreover, the highly dynamic, bursting firing patterns of ORNs cannot be
152 described by the traditional deterministic modeling of neuronal activity. This constitutes a
153 drawback because stochasticity plays a crucial role in shaping firing patterns which are influenced
154 not only by external stimuli but also by the inherent noise involved in channel gating. Therefore, to
155 address the above points realistically, we developed a Langevin formulation of the HH model,
156 which explicitly accounts for the noise introduced by the random opening and closing of ion
157 channels and circadian modulation of the Orco channel conductivity. By integrating channel noise,
158 we could explore how circadian regulation of ionic currents contributes to the variability of firing
159 patterns and how this noise interacts with external stimuli to influence olfactory signal processing.
160 Our model aims to highlight the advantages of using a stochastic framework for modeling the
161 circadian activity of ORNs. The combined experimental and modeling efforts generate a more
162 complete picture and predictions concerning these autonomous processes in sensory neurons,

which are required for future exploration of physiologically relevant anticipatory behaviors that are driven by biological clocks.

4 Methods

4.1 Animals

Nocturnal *M. sexta* hawkmoths were bred and raised from eggs in the rearing facility at the University of Kassel. Males and females were separated during pupal stages. Males were housed isolated from the females to avoid exposure to female pheromones. All experiments were performed with adult males reared in a long-day photoperiod (L:D 17:7 h to prevent diapause) at 25 °C with relative humidity of about 55%. Larvae were fed with an artificial diet modified after Bell and Joachim (1976); adult moths could feed on sugar solution with added vitamins (Roth) *ad libitum* (Riffell et al., 2008).

While all animals were exposed to the same lighting regime as zeitgeber to entrain them up until the start of the experiments, we also attempted pheromone exposure as additional circadian zeitgeber to phase-align spontaneous ORN activity in a subset of males (Ghosh et al., 2024). Without allowing direct contact, virgin males were exposed at zeitgeber time (ZT) 16 to females and naturally occurring pheromone blends in closed mating cages for 30 mins. Males were then moved back into isolation before tip recordings (see below) were started at ZT 17 on the same day. Since we focused on spontaneous spiking activity rather than on pheromone-dependent responses and because repetitive or long pheromone exposure changes the composition of 2nd messenger modulated ion channels in ORNs (Gawalek and Stengl, 2018), we did not employ any further pheromone synchronization protocols.

4.2 Solutions

Ringer compositions were taken from (Pézier et al., 2007) and contained (in mM): 6.4 KCl, 12 $MgCl_2$, 1 $CaCl_2$, 12 NaCl, 10 HEPES, 340 glucose for hemolymph ringer (HLR) at 450 mosmol/kg, and 172 KCl, 3 $MgCl_2$, 1 $CaCl_2$, 25 NaCl, 10 HEPES, 22.5 glucose for sensillum lymph ringer (SLR) at 475 mosmol/kg, both at pH 6.5.

The Orco antagonist OLC15 (N-(4-butylphenyl)-2-((4-ethyl-5-(2-pyridinyl)-4H-1,2,4-triazol-3-yl)thio)acetamide (Chen and Luetje, 2012); kindly provided by Dr. D. Wicher, Max Planck Institute for Chemical Ecology, Jena, Germany) was dissolved in DMSO to a concentration of 100 mM (stock

192 solution stored at 4-8 °C) before being diluted in SLR to a final concentration of 50 µM to be used
193 within one week (stored at 4 °C). We determined in previous studies that, compared to other Orco
194 antagonists, OLC15 is the most specific (Chen and Luetje, 2012; Nolte et al., 2016, 2013; Pask et
195 al., 2013). It is effective at 50 µM, according to dose-response curves, and dose-dependently
196 antagonizes the action of the Orco agonist VUAA1 in intact hawkmoths (Nolte et al., 2016, 2013).
197 DMSO percentage was 0.05% in the final solution.
198 The cAMP analog 8-bromo-cAMP acetoxymethyl ester (8-Br-cAMP-AM; Biolog Life Science
199 Institute GmbH & Co. KG) was dissolved in DMSO to a concentration of 10 mM (stock solution
200 stored at -20°C) and diluted to a final concentration of 100 mM in either SLR or SLR + 50 µM OLC15.

201 **4.3 Electrophysiology**

202 The spontaneous electrical activity of the unstimulated pheromone-sensitive ORNs in a
203 single long trichoid sensillum was recorded extracellularly as *in vivo* tip recording (Kaissling et al.,
204 1987). 1-2-d-old male *M. sexta* that were raised and entrained to zeitgebers as described above
205 were fixed in a custom-made Teflon holder with adhesive tape. The right antenna used for
206 recordings was oriented with its dorsal surface facing up and immobilized near the base with
207 dental wax (Boxing wax strips, KerrHawe SA). Electrodes (Ag/AgCl wire in a glass pipette filled with
208 SLR for the recording electrode and HLR for the reference electrode) were pulled (DMZ-Universal
209 Puller, Zeitz Instruments) from borosilicate capillaries (OD:1.56mm, ID: 1.17mm, without filament;
210 Science Products) to a tip diameter of about 2 µm. All recordings were made at a distance of 2/3 to
211 3/4 of the antenna length towards its distal end because pheromone-sensitive long-trichoid
212 sensilla (sensilla trichodea type 1) occur in a characteristic, homogenous pattern along the
213 hawkmoth antenna (Kaissling et al., 1989; Kalinová et al., 2001; Lee and Strausfeld, 1990).
214 Furthermore, all ORNs in long trichoid sensilla express the same Orco staining pattern (Nolte et al.,
215 2016), share largely overlapping ion channel populations, and obvious differences in the activity of
216 ORNs from different annuli have not been reported (c.f., Dolzer et al., 2003; Gawalek and Stengl,
217 2018; Schneider et al., 2025). Thus, it is very likely that pheromone encoding mechanisms are not
218 locally restricted along the flagellum. Recording and reference electrodes were located on the
219 same annulus: After cutting off the distal 20 annuli of the antenna with micro scissors, the
220 reference electrode was inserted to a depth of 2 annuli into the antennal lumen from the cut end.
221 The cut was covered with electrode gel (GE Medical Systems Information Technology) to prevent
222 desiccation. Under microscopic control, some tips of the long trichoid sensilla of the annulus were

223 cut off with sharpened Dumont forceps, and the recording electrode was slipped over a single
224 sensillum of an upper sensillar row. Electrodes were moved with manual micromanipulators (MMJ,
225 Märzhäuser Wetzlar; and Leitz, Leica Microsystems) or with motorized micromanipulators
226 (Microstar, Scientifica) with a joystick controller (Scientifica).

227 ORN activity was amplified 200-fold (custom built amplifier with 10^{12} Ω input impedance, or
228 ELC-01 MX in combination with DPA-2FX, npi, or EXT 10-2F, npi), low pass filtered at 1.3 kHz,
229 digitized at 20 kHz with a Digidata (1550A or 1550B, Molecular Devices), and saved for offline
230 analysis with Clampex 10 (pCLAMP suite, Molecular Devices).

231 All tip recording experiments were performed at room temperature (21-27 °C) and a relative
232 humidity of 35-60%. These environmental fluctuations across experiments were based on
233 seasonal influences. Throughout each experiment, conditions were stable. To ensure that neither
234 electrode reattachment to the same trichoid sensillum nor application of DMSO influenced spiking
235 activity, we performed two sets of paired experiments at ZT 1-3 in which we recorded the
236 spontaneous activity before and after removing and reattaching the SLR-filled recording electrode
237 to the same sensillum, or recorded the spontaneous activity of the same sensillum in SLR and SLR
238 + 0.15% DMSO. Both treatments did not affect spontaneous spiking activity (Figure 1B).

239 We recorded ORN activity either in long-day conditions (17:7 LD) or constant darkness (DD)
240 to examine the free-running peripheral ORN clock. For LD experiments, the light regime continued
241 as in the rearing facility during the experiment. For DD and OLC15 experiments, the lights were
242 turned off at the beginning of the recording, i.e., all animals were exposed to the same light
243 zeitgeber until the beginning of the experiment. To examine the effect of Orco on the spontaneous
244 action potential (AP) activity pattern, we used the recording electrode to infuse OLC15 in DD
245 conditions. To examine the effect of cAMP on Orco gating, we recorded the spontaneous ORN
246 activity at the end of the moth's activity phase (ZT 1-3) in SLR as control, and either 8-Br-cAMP-AM,
247 or 8-Br-cAMP-AM + OLC15, infused through the recording electrode.

248 ORNs generate spontaneous APs. However, high spiking activity during control recordings is
249 indicative of stress, whereas low/no activity could be indicative of damage. Therefore, we only
250 considered experiments in which the average spiking frequency was between 2 Hz and 0.008 Hz in
251 control conditions.

4.4 Data analysis

To characterize the spontaneous ORN spiking activity, we first detected spikes with a self-written program in Python. Using the scipy.signal package and find_peaks function, we used a moving mean with 100 samples (5 ms) window size for baseline correction, followed by applying a 8th order low-pass Bessel filter (2000 Hz cutoff frequency) to the raw voltage trace to facilitate spike detection within the following conditions: spike full width (3-15 ms), threshold search for amplitude of spike (0.5-2.5 mV) and threshold prominence (0.1). Two or more consecutive spikes with intervals ≤ 50 ms were considered a burst (Dolzer et al., 2001). We then calculated the following attributes in bins of either 10 min or 1 h for further analysis: instantaneous spike frequency (ISI, 1 / inter-spike interval), inter-burst interval (IBI, time between two consecutive bursts with no single spikes in between), inter-event interval (IEI, time between two events, i.e. two consecutive single spikes, two consecutive bursts, a burst and a consecutive spike, and vice versa), burst duration (time from first to last spike in a burst), percentage of all spikes in the experiment that are members of burst, and mean number of spikes per burst (Figure 1A). All statistics were done with those binned values.

Hawkmoth behavioral and physiological rhythms desynchronize across the population in the absence of zeitgebers like circadian rhythms of pheromone stimulation and daily light-dark cycles. Therefore, we first used RAIN analysis (Thaben and Westermark, 2014) to identify circadian rhythms (24 ± 4 h) in the attributes above for each animal and condition (LD, DD, OLC15) in the 1 h-binned data. Data was downsampled to 2 h resolution and thus included every other 1 h bin to speed up computational time. To further quantify the circadian changes in attributes across animals, it was then necessary to phase align the recordings obtained in DD and OLC15. To achieve this, we used an optimization procedure to calculate the optimal temporal lags for each dataset, aiming to maximize the overall cross-correlation between the calculated binned spike frequency series. The optimization was performed using simulated annealing, which provided a set of time shifts (lags) for each series. These lags were applied to shift the frequency data in a manner that maximized the synchronization between the different subjects' data, resulting in a "subjective ZT" with subjective ZT 0 at the first maximum of the binned ISI for each individual. The objective function used for optimization was the negative sum of pairwise correlations between all series after applying the shifts. The resulting alignment allowed us to compare the frequency patterns across the different conditions.

283 Once the data were aligned, we computed the mean frequency across all subjects for each
284 bin and each condition. Then, the first high activity period was identified by finding the maximum in
285 the mean frequency series. Subsequently, we identified the second high activity period as the time
286 24 hours after the first one and the first low activity period was found by locating the minimum in
287 the mean frequency series between the two high activity periods. Besides the mean frequency, we
288 also searched for significant oscillations in IBI, IEI, burst duration, percentage of spikes that are
289 part of bursts, and mean number of spikes per burst. For this we found the maximum value of these
290 statistics within a 3 h range centered in the first low activity period and compared it with the values
291 at the second high activity period.
292 Continuous wavelet and Fourier analysis were performed using PyBoat (version 0.9.12)
293 (Mönke et al., 2020) to examine the time series of neuronal firing frequency. The continuous
294 wavelet method allows us to detect and characterize rhythmic patterns within the data by
295 identifying frequency components that change over time. Specifically, we used wavelet analysis to
296 determine whether a neuron exhibited circadian and ultradian rhythms. Unlike traditional Fourier
297 analysis, which provides an overall frequency composition but assumes stationarity, wavelet
298 analysis is particularly useful for biological signals because it can reveal how these frequencies
299 evolve dynamically. By applying this approach, we could assess not only the presence of ultradian
300 rhythms but also whether their strength or occurrence fluctuated in a circadian manner, indicating
301 modulation by the 24-hour cycle. For this analysis, we used the 10 min-binned data to have
302 sufficiently high resolution to detect ultradian rhythms. Periods were determined as local maxima
303 in the Fourier power spectra.

304 4.5 Real-time quantitative polymerase chain reaction (qPCR)

305 We followed the qPCR methodology detailed in (Schneider et al., 2025). Briefly, male moths
306 were isolated and cultured until the second day after eclosion, and the antennae from four
307 individuals were collected every 4 hours for one day, starting at ZT 0, using liquid nitrogen, with four
308 biological replicates per time point. Total RNA was extracted using TRIzol® Reagent (Invitrogen) and
309 quantified for concentration and purity with the NanoDrop ND-1000 spectrophotometer (Thermo
310 Fisher Scientific). First-strand complementary DNA (cDNA) was synthesized using the PrimeScript™
311 RT reagent Kit with gDNA Erase (Takara Bio Inc.). Primers for *Orco* (F: GCTCGCTACCACCAAATTGC,
312 R:TCGTGACCCAACTGACAACA; Gene ID: LOC115452348) and for *timeless* (*tim*) (F:
313 TTAAGCCGACCGTAGTGCTG, R: CGTCTTCCGTCCATGTGTCT; Gene ID: LOC115446009) were

314 designed using the Primer-BLAST online program of NCBI. The qPCR was conducted following the
315 protocol of TB Green® Premix Ex Taq™ II (Tli RNase H Plus) (Takara Bio Inc.), with the program: 95 °C
316 for 30 s, followed by 40 cycles of 95 °C for 5 s, and 60 °C for 30 s. Relative expression levels of *Orco*
317 were calculated using the $2^{-\Delta\Delta Ct}$ method (Livak and Schmittgen, 2001).

318 **4.6 Statistics**

319 All statistics were done with self-written python codes, SigmaPlot 12 (Systat Software), or
320 JASP (versions 0.19.03 and 0.95.4, University of Amsterdam) with a significance level $\alpha = 0.05$.
321 Unless noted otherwise, data were checked for normal distribution with Anderson-Darling or
322 Shapiro-Wilk tests and for equal variance with Levene's test. If one of these assumptions failed, we
323 used non-parametric tests, otherwise we used parametric tests.
324 To assess the statistical significance of observed differences in neuronal activity of the
325 aligned data between ZTs, we applied the Wilcoxon signed-rank test to pairwise comparisons
326 between the first low activity period and the subsequent high activity period and discarded the
327 transient high activity at the beginning of most recordings.
328 For paired recordings (electrode reattachment, addition of DMSO, or cAMP/cAMP+OLC15 in
329 the same animal, we used either paired student-t test or Wilcoxon signed-rank test, depending on
330 normal distribution of data.
331 For other data, we used an ANOVA on ranks with either Tukey's or Dunn's post-hoc test for
332 multiple comparisons as indicated.

333 **4.7 ORN Model**

334 In this study, we introduce a single-compartment Hodgkin-Huxley (HH) type model of the
335 spontaneous activity of *M. sexta* ORNs (available on GitHub (Forlino et al., 2025)). The model
336 contains 5 sets of ion channels that were previously identified in electrophysiological recordings
337 (Dolzer et al., 2021): the fast sodium (Na^+) and potassium (K^+) channels responsible for the
338 generation of spikes, low voltage-activated calcium channels (LVA) responsible for the initiation of
339 bursts, calcium-gated potassium channels (BK) responsible for the termination of bursts, and the
340 Orco channel, which is a voltage-independent non-specific, cAMP-gated channel. A schematic of
341 the model is provided in Figure 2A. We modeled Orco as a ZT-dependent conductance to represent
342 the effect of the oscillations in cAMP concentration that were identified in both hawkmoth and
343 cockroach antennae (Schendzielorz et al., 2014, 2015, 2012) (Figure 2B, C). For simplicity we chose
344 to use a sine function to directly represent the oscillations in Orco conductivity, but similar results

can be achieved by modeling it as an output of a Goodwin model of the circadian clock via cAMP concentration.

Each type of ion channel possesses one or more gates that can open and close individually with transition rates α and β for opening and closing, respectively, of activation gates (n, m) and inactivation gates (h). As a result, each possible combination of open and closed gates defines a possible state in which each ion channel can be found. A schematic of the Markov chain depicting all possible states and transitions for each ion channel is shown in Figure 2D. Each ion channel can conduct current only in the state where all its gates are open.

First, we constructed a deterministic 22-dimensional model to serve as the mean field of the Langevin model following the methodology proposed by Pu and Thomas (2020). Here, one dimension tracks the membrane potential, another the intracellular Ca^{2+} concentration, and the remaining 20 dimensions track the number of channels that are in a specific state of the Markov chains. Considering the conservation of the total number of ion channels, each type of ion channel required one less dimension than the total possible states.

The complete Langevin model adds to the mean field an independent noise source for each transition in the Markov chain. These noise sources are biophysically motivated since the transition between ion channel states is a stochastic process, with the probability of transition determined by the kinetics of each kind of ion channel. The variability in the spiking behavior of a neuron emerges from this non-deterministic gating of individual ion channels. The detailed mathematical description of the model can be found in the Supplementary Material.

5 Results

We tested the hypothesis that sensory neurons, such as insect ORNs, perform active, anticipatory sensing based upon an endogenous plasma membrane clock with the pacemaker channel Orco as the core element. We focused on pheromone-sensitive long trichoid sensilla of male *M. sexta* hawkmoth antennae which express daily rhythms in pheromone sensitivity and temporal resolution that are controlled by a circadian clock. We performed minimally invasive *in vivo* tip recordings over the course of several days to search for daily rhythms in spontaneous spiking activity as a measure of endogenous membrane potential oscillations.

373 **5.1 Pheromone-sensitive hawkmoth ORNs exhibit Orco-dependent circadian**
374 **rhythms in spontaneous spiking activity**

375 The ORNs that innervate the pheromone-sensitive long trichoid sensilla on male *M. sexta*
376 antennae display spontaneous spiking patterns of irregular bursts with interspersed single action
377 potentials in short-term recordings (Dolzer et al., 2001). In the present study we documented the
378 same pattern in long-term recordings over the course of 2-7 days. This enabled us to search for
379 daily and circadian rhythmicity in spontaneous ORN spiking activity in the absence of pheromone
380 stimulation.

381 RAIN analysis of the spontaneous spiking patterns revealed significant daily rhythms in 7 of
382 11 animals under long-day conditions (17:7 h LD) (Figure 3A). The maxima in spontaneous activity
383 occurred mostly during the dark phase when nocturnal hawkmoths are active (Figure 3A (top), Bi
384 light blue arrow), and minima occurred during the light phase when hawkmoths rest/sleep (Figure
385 3A (bottom), Bi dark blue arrow). High spiking activity in the dark phase had a mean maximum
386 frequency of ~3 Hz (delta range: 0.5 – 4 Hz) (Figure 3Bii). In contrast, the minimum spiking
387 frequencies during the hawkmoth's resting phase were below 0.5 Hz (Figure 3A (bottom)).

388 Since ORN firing patterns had a clear daily rhythm in LD both in individual animals (Figure
389 3Bi) and averaged across animals (Figure 3Bii, Biii), we examined whether these rhythms depended
390 on cycling light cues or whether they persisted in constant darkness (DD), as expected for an
391 endogenous, circadian clock-driven rhythm. In DD, the spontaneous ORN firing pattern remained
392 rhythmic (RAIN: 8 of 12 animals), albeit with less robustness: The single peak of high spiking activity
393 that was observed at the same ZT across several days in LD divided into multiple bouts of high
394 spiking activity in the activity phase in 8 of 12 animals (Figure 3Ci). Also, in DD conditions, the high
395 spiking activity phase shifted into the subjective day due to the individual endogenous circadian
396 periods of about 23.5 +/- 2.8 h (21.27 h in Figure 3Ci). Using pheromone exposure as additional
397 zeitgeber also did not synchronize the animals (Figure 3 – Supplement). Thus, averaging the
398 instantaneous spiking activity across all DD animals did not depict clear circadian rhythms (Figure
399 3Cii). Therefore, we phase-aligned the mean frequency of spontaneous activity (see Methods).
400 After alignment, circadian rhythms were visible across DD animals (Figure 3Ciii), comparable to the
401 daily rhythms in LD (cf. Figure 3 Biii and Ciii).

402 Next, we examined whether Orco, a leaky, non-specific cation channel, is the dominant
403 depolarizing pacemaker current of ORNs that drives circadian rhythms in spontaneous spiking
404 activity. Infusion of the Orco antagonist OLC15 into the sensillum lymph obliterated circadian

405 rhythms and attenuated the spontaneous activity in several, but not all experiments (RAIN: 2 of 12
406 animals expressed circadian rhythms) (Figure 3Di). This attenuation resulted in a linear decrease in
407 spiking activity over several days (Figure 3Dii, Diii). Even after phase-aligning the individual
408 experiments, no circadian rhythm was present in the average across all OLC15-treated animals
409 (Figure 3Diii).

410 Because OLC15 is not membrane-permeable on its own it was infused with low
411 concentrations (0.05%) of DMSO through the recording electrode into the sensillum lymph and,
412 therefore, effectiveness increased over time. Hence, we fit the spiking activity of each animal and
413 in each condition with linear regression lines over the whole recording time to compare the slopes
414 of the fits (Figure 3E). In LD, the mean ± SD slope was 0.004 ± 0.006 Hz/h, indicating that the
415 average spiking activity remained similar throughout the duration of the recording. In DD, the slope
416 was -0.003 ± 0.018 Hz/h and was not different from LD. In contrast, the mean slope during OLC15
417 treatment was -0.007 ± 0.022 Hz/h, significantly smaller than in LD (ANOVA on ranks with Dunn's
418 post-hoc test; $H(2) = 7.681$, $p = 0.021$). The negative slope corroborated the finding that spiking
419 activity decreased over time in the presence of the Orco blocker.

420 Activity rhythms between hawkmoths desynchronize and have only weak phase coupling in
421 the absence of pheromone stimulation, even in LD cycles (Ghosh et al., 2024). Therefore, we first
422 determined the percentage of animals that expressed circadian rhythmicity (period of 24 ± 4 h) for
423 each attribute with RAIN (Figure 4A). In LD, all attributes except #AP per burst and intra-burst
424 frequency showed daily modulation in most animals. Circadian rhythms were still present in more
425 than half of the animals in DD for mean spiking frequency, mean burst frequency, and mean event
426 frequency. In contrast, the attributes of only a few animals remained rhythmic with the Orco
427 channel blocker OLC15.

428 To further quantify the circadian differences, especially of the desynchronized animals, we
429 compared different attributes of spontaneous activity between periods of high and low activity, for
430 DD conditions after phase alignment (see Methods) instead of comparing fixed ZT or circadian time
431 (CT) intervals. Despite the high variability in ORN spiking between individuals, the mean frequency
432 of spontaneous ORN activity was significantly higher during the high activity phase than during low
433 activity in both LD and DD recordings (Figure 4Bi, Bii). In LD, but not in DD, the frequency of bursting
434 increased significantly during the high activity phase (Figure 4Ci, Cii). The percentage of spikes that
435 are part of bursts was less variable and lower during the high activity phase in LD but not
436 significantly different in DD (Figure 4Di, Dii). The mean burst duration was less variable during the

437 high than the low activity phase in LD, but not significantly shorter in any condition (Figure 4Ei, Eii).
438 Furthermore, both in LD and DD, the mean inter-event frequencies were significantly higher during
439 the high activity phase (Figure 4Fi,Fii), indicating a significantly higher overall spontaneous spiking
440 activity during the hawkmoth's activity phase. The mean number of spikes per burst, and intra-
441 burst frequencies did not differ significantly between high or low activity periods in both LD and DD
442 conditions (Figure 4Gi, Gii, Hi, Hii). The addition of Orco antagonist OLC15 deleted any significant
443 differences of spontaneous activity found in LD and DD (Figure 4Biii-Hiii). In conclusion, the mean
444 frequency of spontaneous spiking and the frequency of bursting expressed circadian modulation,
445 and are both most likely controlled via a circadian clock that involves Orco.

446 **5.2 Orco imposes circadian modulation on the ultradian rhythms in spontaneous**
447 **ORN activity**

448 After establishing that Orco influences the circadian changes in ORN spiking activity between
449 the animal's resting and activity phase we examined if Orco also influences ORN spiking rhythms
450 on the largely different ultradian timescales in the frequency range between 0.01-1000 Hz. In all
451 conditions, two broad bands of ultradian instantaneous frequencies were evident: one upper band
452 of >10 to ~100 Hz (beta/gamma range) and a lower band between 0.1 to ≤10 Hz (delta/theta/alpha
453 range) (Figure 5). The upper band primarily represents the frequencies of spikes within a burst,
454 while the lower band represents single spikes and frequencies between bursts.
455 In LD, two types of daily/circadian modulation of the ultradian frequencies occurred (Figure
456 5A). The upper frequency band was mostly modulated in prevalence (its frequency of occurrence)
457 but not in its frequency range. The lower band was modulated both in prevalence and frequency
458 range, which resulted in a sinusoidal change in the mean of the frequency band over 24 h. During
459 the hawkmoth's activity phase, higher frequencies of up to ~10 Hz occurred, while frequencies
460 dropped below 1 Hz during the resting phase. Because of this circadian increase in the lower
461 frequency band, it merged with the high frequency band when both bands had maximum
462 prevalence during the activity phase around ZT 0.
463 The circadian modulation of both frequency bands was maintained in constant darkness
464 (Figure 5B) but phase-shifted with respect to the projected ZT due to the endogenous circadian
465 period of each individual. Again, this indicates that a clock is modulating the spontaneous ORN
466 spiking activity over the course of a day. The addition of the Orco antagonist OLC15 deleted any
467 circadian modulation of either frequency band. Interestingly, the instantaneous frequencies in

both bands still showed correlated changes in prevalence and merging, but now at ultradian periods only.

Additional Fourier analysis (see Methods) of spontaneous spiking activity over the course of several days revealed faster ultradian and slower infradian rhythms, ranging from 0.6 h to 38 h, in addition to the circadian (24 ± 4 h) rhythm (Figure 6Ai, Bi, Ci). Some rhythms (factorials of 24 h, like 12 h, 6 h, etc.) appeared to be harmonics of the circadian rhythm, which were not excluded in our analysis. Most animals expressed ultradian rhythms of 2-4 h in LD as well as DD conditions. Fourier confirmed the decrease of animals with circadian spiking activity in OLC15 (58.3% in DD, 33.3% in OLC15). Please note that discrepancies in the number of animals with circadian rhythms between RAIN and Fourier/wavelet analyses are due to the fundamentally different sensitivities in methodology. In brief, Fourier analysis assumes a stationary sinusoidal component, whereas RAIN as a rank-based umbrella test detects consistent raise-fall patterns, including asymmetric rhythms. Nonetheless, both methods confirmed a dramatic decrease in animals with circadian spiking patterns in OLC15. In addition, 33.3% of animals expressed infradian spiking patterns (up from 0% in DD) with OLC15. Ultradian periods could be detected in all animals in all conditions but their distribution did not differ between conditions (1-way ANOVA;$F(2, 117) = 0.87$, $p = 0.421$). These results were corroborated by continuous wavelet analysis, which provided time-resolved spectral power across different rhythmic periods (Figure 6Aii, Bii, Cii).In control LD and DD conditions, wavelet power for ultradian periods increased during times of elevated firing rate and decreased during periods of low activity (Figure 6Aii and Bii, middle and bottom panels). This dynamic pattern indicates that ultradian rhythms were not constant over time but were instead modulated with a circadian rhythm, becoming more prominent during circadian peaks in neuronal activity. Such circadian gating of ultradian power was clearly visible in the wavelet spectrograms as alternating bands of higher and lower ultradian power aligned with daily activity cycles. Following Orco blockade with OLC15, this modulation was disrupted (Figure 6Cii middle panel): although ultradian components persisted (Figure 6Cii bottom panel), they no longer showed systematic variation with the circadian cycle, suggesting a decoupling of ultradian rhythms from circadian control.

5.3 Orco expression is not under the control of the molecular TTFL clockwork

So far, our results indicated a prominent role of Orco in the circadian modulation of ORN spiking activity. Since it is the general opinion that the master circadian clock is the TTFL clock that

499 dominates all physiological and behavioral circadian rhythms via transcriptional control, we
500 examined whether Orco transcript abundance shows a daily rhythm, as previously found for clock
501 genes in hawkmoth antennae (Schneider et al., 2025; Schuckel et al., 2007). However, in contrast
502 to the circadian clock gene *tim*, qPCR of whole male hawkmoth antennae across different ZTs
503 revealed no significant daily rhythm of Orco transcript abundance (Figure 7; ANOVA on ranks,
504 $H(5) = 6.91$, $p = 0.227$). Thus, we suggest that Orco function is controlled via a posttranslational
505 circadian clockwork mechanism that is associated directly with the plasma membrane (Stengl and
506 Schneider, 2024; Stengl and Schröder, 2021).

507 5.4 Circadian changes in Orco conductance are sufficient to modulate spiking 508 activity in a computational model of a hawkmoth ORN

509 The maximum conductivity of *Drosophila* Orco as a leaky ion channel is modulated by cAMP
510 (Getahun et al., 2013; Martín et al., 2001; Sargsyan et al., 2011; Wicher et al., 2008). In hawkmoth
511 antennae, cAMP levels oscillate throughout the day and are involved in sensitizing the ORNs to
512 pheromone (Dolzer et al., 2021; Flecke et al., 2010; Flecke and Stengl, 2009; Schendzielorz et al.,
513 2014, 2015). Hence, cAMP modulation of Orco conductance could be a putative mechanism for
514 the Orco-dependent circadian modulation of ORN spiking activity, integrating Orco in a circadian
515 PTFL based membrane clockwork (Stengl and Schneider, 2024).

516 To test the hypothesis that Orco is a cAMP-dependent, leaky ion channel, we constructed an
517 ORN model (Methods and Supplementary Material) and tuned the parameters to provide a
518 quantitative match with the biological data. The developed model provides a unified description of
519 experimental observations. For instance, the ORN model yields irregular spiking activity with a
520 bimodal distribution, consisting of both bursts and isolated spikes, successfully reproducing the
521 experimental recordings (Figure 8A). This suggests a unified mechanism underlying the initiation of
522 both phenomena: If the pacemaker-driven depolarization reaches the Na^+ threshold a firing
523 process begins, and at this point randomness determines if other slower ion channels responsible
524 for bursting are sufficiently activated to sustain a burst of several spikes.

525 Additionally, the ORN model replicates the distribution of the number of spikes per burst,
526 which follows a decreasing exponential trend in both experimental and simulated results (Figure
527 8B).The model also successfully reproduces the circadian modulation of spiking activity: the
528 maximum firing rate occurs when the Orco conductance is maximal, whereas the maximum

percentage of spikes that are part of bursts correlates with the lowest Orco conductance, resulting in antiphase oscillations, as were observed in the experimental recordings (Figure 8C).

The frequency prevalences in the model over several days clustered in two distinct frequency bands: an upper band that corresponds to the intra-burst frequencies and a lower band, corresponding to inter-burst frequencies (Figure 8D), in agreement with the biological experiments (Figure 5A, B). When circadian oscillations in Orco conductance were included, inter-burst frequencies showed significant circadian variations, whereas intra-burst frequencies remained relatively constant, reminiscent of the biological data. Notably, the simulation captured the experimentally observed "merging" effect, where the low frequency band approaches the top band during high-activity periods (Figure 8D).

This merging of spiking and bursting frequencies suggests that the system approached a bifurcation, transitioning from a bursting regime to tonic spiking activity. Further evidence for the near bifurcation condition of the neurons is the distribution of number of spikes per burst that followed a decreasing exponential trend in contrast to a constant value, or a bounded range of spikes per burst, which would be expected from a standard bursting neuron model (Figure 8B). The observation that the circadian modulation of spiking activity requires only one parameter, namely changes in the Orco conductivity, to describe the circadian effects on the ORN spiking pattern indicates the crucial role of the Orco channel in circadian control.

5.5 cAMP regulates the circadian function of Orco

Our computational model predicted that the daily/circadian oscillations in cAMP levels (Schendzielorz et al., 2015) control the circadian modulation of spontaneous spiking activity of hawkmoth ORNs. To test this prediction in hawkmoth ORNs, we increased cAMP levels by infusing 8-Br-cAMP-AM through the recording electrode into the sensillar lymph (Figure 9) at ZT 1-3. This significantly increased the mean frequency of the spontaneous spiking activity (Figure 9A; Wilcoxon signed-rank test $Z = -2.701$; $p = 0.004$). To check whether this increase in mean frequency was caused by direct or indirect interaction of cAMP with the Orco channel, we infused the Orco antagonist OLC15 together with 8-Br-cAMP-AM through the same recording electrode. Blocking Orco prevented a significant change in the spontaneous spiking frequency via the cAMP analogue (Figure 9B; paired t-test $t(9) = -1.446$; $p = 0.182$). This further corroborates cAMP-dependent modulation of the circadian pacemaker channel Orco.

6 Discussion

With *in vivo* long-term tip recordings of pheromone-sensitive long trichoid sensilla of male *M. sexta* hawkmoth antennae, we searched for a membrane-associated PTFL clockwork component that orchestrates membrane potential oscillations to facilitate active sensing of pheromone patterns during mating flights. Indeed, we detected interlinked circadian and ultradian frequencies in the spontaneous spiking activity, indicative of underlying membrane potential oscillations in ORNs. We found that the olfactory receptor co-receptor (Orco) acts as a pacemaker channel that controls the circadian modulation of the spiking activity without affecting the ultradian frequency ranges that are relevant for the primary fast, phasic pheromone response (Dolzer et al., 2003; Nolte et al., 2016; Schneider et al., 2025). Our computational model confirmed that the circadian modulation of open-time probability of Orco as a leaky pacemaker channel was sufficient to account for our experimental results. Since Orco was not under circadian transcriptional control of the TTFL present in hawkmoth ORNs, our findings are consistent with our novel hypothesis that the ORN's plasma membrane constitutes an endogenous, plastic post-translational feedback loop (PTFL) clockwork. Consistent with experimental data (Schendzielorz et al., 2015), we propose that PTFL-generated endogenous multiscale membrane potential oscillations comprising interlinked oscillations in Ca^{2+} and cAMP levels provide circadian modulation of Orco conductance rather than TTFL-commanded circadian Orco transcription and turnover.

The expression of a 2nd messenger-dependent pacemaker/leak channel in ORNs that does not require daily transcription would constitute an economic and rapidly adjustable mechanism of active sensing. It could generate endogenous membrane potential oscillations that are tuned to detect and resonate with behaviorally relevant temporal patterns of zeitgeber signals, such as the circadian and ultradian pheromone fluctuations in the insect's environment (Stengl and Schneider, 2024; Stengl and Schröder, 2021). The present study provides the first evidence for a systems view of biological timing that involves a PTFL membrane clock in insect sensory neurons, instead of the prevailing hierarchical view that assumes all endogenous circadian oscillations are outputs of the genetic TTFL clock (Stengl and Schneider, 2024; Stengl and Schröder, 2021).

6.1 Orco acts as a pacemaker channel that controls membrane potential oscillations underlying spontaneous ORN spiking activity

The resting membrane potential of most silent neurons lies close to the negative equilibrium potential for potassium ions, mainly due to potassium leak channels (Goldstein et al., 2001; Hille,

590 2001; Patel and Honoré, 2001; Talley et al., 2001). Spontaneously active neurons require the
591 expression of leak or pacemaker channels that open at the hyperpolarized resting membrane
592 potential, thus depolarizing the neuron(Bose et al., 2014; Cochet-Bissuel et al., 2014; Das et al.,
593 2016; Golowasch et al., 2017; Lüthi and McCormick, 1998; Ratliff et al., 2021; Robinson and
594 Siegelbaum, 2003; Sharma et al., 2023). When the pacemaker-driven depolarization reaches spike
595 thresholds, voltage-gated Na^+, K^+ and Ca^{2+} channels promote Ca^{2+} influx and spiking. Voltage- and
596 Ca^{2+}-gated hyperpolarizing K^+ channels then repolarize the neuron to negative membrane
597 potentials, re-starting the cycle. Thus, membrane potential oscillations with interlinked oscillations
598 in intracellular Ca^{2+} levels drive spontaneous spiking activity which depends on the type of
599 pacemaker channel and antagonistic ion channels present.

600 In insect ORNs, at least two types of pacemaker channels exist: the highly conserved, slow,
601 leaky Orco, which we focus on in this study, and an inversely voltage-dependent HCN type channel
602 (Butterwick et al., 2018; Dolzer et al., 2021; Kodirov, 2022; Lee and MacKinnon, 2017; Mandala et
603 al., 2025; Nolte et al., 2016, 2013; Sato et al., 2008; Stengl and Funk, 2013; Stengl and Schneider,
604 2024; Stengl and Schröder, 2021; Wicher et al., 2008; Wicher and Miazzi, 2021). When expressed *in*
605 *vitro* in heterologous expression systems, *Drosophila* as well as *Manduca* Orco homo- and
606 heteromers assemble into leaky, non-specific cation channels with a reversal potential around 0
607 mV, constitutively leaking Na^+, K^+, and Ca^{2+} into ORNs (Nolte et al., 2016, 2013; Sato et al., 2008;
608 Stengl and Funk, 2013; Wicher et al., 2008; Wicher and Miazzi, 2021). Thus, while this study did not
609 aim to unravel the overall generation of spontaneous activity in ORNs, here, we examined whether
610 the leak channel Orco in hawkmoth ORNs is the core pacemaker channel responsible for
611 membrane potential oscillations that drive spontaneous circadian activity (Stengl, 2010; Stengl
612 and Schneider, 2024).

613 Differential location and function of Orco homo-or heteromers in the distinct membrane
614 compartments of ORNs that face different ionic environments appear likely (Stengl and Funk, 2013;
615 Stengl and Schröder, 2021). We propose that homomeric *Manduca* Orco pacemaker channels, as
616 core element of a PTFL membrane clock, are restricted to the soma/inner dendrite compartment of
617 ORNs (Stengl and Schneider, 2024; Stengl and Schröder, 2021). In contrast, we expect *Manduca*
618 Orco heteromers to serve as obligatory chaperons to maintain ORs in the ciliary membranes, as
619 proven in *Drosophila* (Benton et al., 2006). Since the ciliary compartment faces very high
620 concentrations of K^+ in the sensillum lymph, matching intracellular K^+ levels (Kaissling and
621 Thorson, 1980; Steinbrecht, 1992), we propose that Orco in ciliary membranes remains closed via

622 unknown mechanisms, while Ca^{2+} channels of the TRP ion channel family serve the primary events
623 of pheromone transduction (Gawalek and Stengl, 2018; Stengl, 1994, 1993). Otherwise, Orco
624 channel opening would clamp the ciliary membranes at 0 mV, strongly reducing the driving force of
625 pheromone-dependent receptor currents, not allowing for the ORN's extreme pheromone
626 sensitivity (Stengl and Funk, 2013).

627 In support of this hypothesis, in both *Drosophila* (Benton et al., 2006) and *Manduca* (Nolte et
628 al., 2016), Orco antisera labeled Orco in two of the three sealed off ORN membrane
629 compartments: in the membranes of soma/ inner dendrite compartment, as well as in the
630 membrane of outer cilia, but not in the axons of ORNs. In contrast, antisera against an OR in
631 *Drosophila* detected ORs only in ciliary membranes but not in the other compartments of ORNs.
632 Thus, the colocalization of OR-Orco heteromers only in cilia confirm that Orco is an obligatory
633 coreceptor and chaperone of ORs localizing and maintaining the OR-Orco complexes in the ciliary
634 membrane (Benton et al., 2006). Since antisera against *Manduca* ORs are not available, we do not
635 known whether the pheromone-sensitive OR-Orco heteromers are solely located to ciliary
636 membranes also in the hawkmoth while Orco homomers are found in the soma/inner dendrite
637 compartment (Fandino et al., 2019). However, we know that Orco exists as homomeric complexes
638 in wild-type hawkmoth ORNs because Orco expression starts during development well before ORs
639 are present and because Orco agonist VUAA1 activates Orco in primary cell cultures of not yet
640 pheromone-sensitive maturing ORNs (Nolte et al., 2016; Schweitzer et al., 1976).

641 In summary, we propose Orco to be a 2nd messenger cascade-dependent core element of a
642 PTFL membrane clock that is located in the soma/inner dendrite compartment of ORNs, which
643 controls the ORN's membrane potential and is coupled to - but not dominated by - the TTFL clock
644 in the hawkmoth ORNs (Schuckel et al., 2007; Stengl and Schneider, 2024).

645 6.2 Orco is suggested to be a second messenger-dependent control hub of a PTFL 646 membrane clock that regulates circadian membrane potential oscillations in 647 hawkmoth ORNs

648 Different 2nd messenger cascades regulate *Drosophila* Orco via Ca^{2+}/calmodulin and via
649 phosphorylation/de-phosphorylation at multiple sites (Cao et al., 2016; Getahun et al., 2016; Guo
650 and Smith, 2017; Mukunda et al., 2016, 2014; Sargsyan et al., 2011). The Ca^{2+}/calmodulin binding
651 site controls the localization of the OR-Orco complex in the ciliary membrane of ORNs, provides for
652 negative feedback control of Orco conductance, and depends on previous odor stimulation (Bahk

653 and Jones, 2016; Cao et al., 2016; Guo and Smith, 2022; Jain et al., 2021). After phosphorylation of
654 Orco by protein kinase C (PKC), Orco directly or indirectly becomes cyclic nucleotide-dependent,
655 with cGMP and cAMP increasing its open-time probability (Getahun et al., 2013; Wicher et al.,
656 2008). While we do not know the second messenger-dependent modulation of hawkmoth Orco,
657 due to Orco's highly conserved structure we assume similar Ca^{2+}/calmodulin-, PKC-, and cyclic
658 nucleotide-dependent control of Orco's localization and open-time probability.
659 Since blocking Orco in *M. sexta* decreased the spontaneous activity and deleted its circadian
660 but not ultradian modulation, Orco is apparently the main target for modulation of circadian
661 activity in hawkmoth ORNs. The ultradian rhythms in spontaneous activity are presumably
662 controlled by additional pacemaker channels. Since Orco transcript abundance was constant
663 throughout the day, Orco is not controlled directly by the circadian TTFL clock. Rather, a self-
664 assembling PTFL membrane clock controls open-time probability and/or membrane localization of
665 Orco via posttranslational modifications in a circadian manner. Because circadian rhythms in
666 cAMP levels and phase-leading circadian rhythms in IP_3 were found in hawkmoth antennae
667 (Schendzielorz et al., 2015), it is likely that Orco's phosphorylation state regulates its cAMP
668 dependence in a daily rhythm. Indeed, our results showed that the increase of spontaneous activity
669 caused by 8-Br-cAMP application is canceled with co-application of the Orco blocker OLC15. Thus,
670 we assume that a PTFL membrane clock determines the circadian oscillations in the pheromone
671 sensitivity and temporal resolution of ORNs via Ca^{2+}, PKC, and cAMP-dependent membrane
672 potential control (Dolzer et al., 2021, 2008; Flecke et al., 2010, 2006; Redkozubov, 2000;
673 Schendzielorz et al., 2015, 2012; Ziegelberger et al., 1990).
674 Our hypothesis that a circadian PTFL membrane clock in hawkmoth ORNs controls circadian
675 rhythms in spontaneous spiking activity predicts that this PTFL clock comprises a membrane
676 signalosome with the pacemaker channel Orco as central control hub (Stengl and Schneider,
677 2024). In the soma/inner dendrite compartment of the ORNs the protein complexes of this PTFL
678 signalosome would generate the specific ultradian and circadian frequencies of endogenous
679 potential oscillations, linked to oscillations of Ca^{2+} and cAMP that determine physiological
680 setpoints of the ORN during circadian sleep-wake cycles. Thus, the PTFL membrane clock that
681 generates endogenous membrane potential and Ca^{2+} level oscillations minimally consists of
682 depolarizing, Ca^{2+} permeable Orco, voltage-gated Ca^{2+}, and hyperpolarizing K^+ channels. In the
683 same PTFL soma clock, membrane-anchored adenylyl cyclases (ACs) and phosphodiesterases
684 (PDE), that are antagonistically controlled by intracellular Ca^{2+} levels, are proposed to generate

685 circadian cAMP oscillations (Halls and Cooper, 2011). Kinases, such as PKC and PKA, could couple
686 potential oscillations with cAMP oscillations that target Orco, phosphatases, and PDEs via
687 negative feedback. Very likely, this membrane PTFL clock is interlinked with metabolic clocks such
688 as PTFL clocks that generate endogenous rhythms of redox elements or ATP availability (Edgar et
689 al., 2012), as evident in, e.g., human red blood cells, which lack a nucleus (O'Neill and Reddy,
690 2011).

691 Furthermore, this PTFL-clock could contain octopamine receptors that couple to
692 endogenous oscillations of intracellular Ca^{2+} and cAMP levels through activation of $G_{\alpha o}$ and $G_{\alpha s}$, as
693 found in hawkmoths (Dacks et al., 2006; Flecke et al., 2010). Since octopamine levels in the
694 hemolymph exhibit circadian oscillations and octopamine sets a physiological state of heightened
695 alertness in insects, the circadian PTFL clock in ORNs would synchronize with endogenous
696 physiological rhythms via octopamine receptor activation (Flecke and Stengl, 2009; Schendzielorz
697 et al., 2015). This also constitutes a possible pathway to synchronize the ORN PTFL clock with
698 circadian TTFL clocks in both ORNs and the brain. In horseshoe crab, the master clock sends
699 multiscale patterned spike trains through retinal efferents at night, which carries information about
700 the circadian phase and enhances visual sensitivity based on octopamine release and cAMP
701 signaling (Battelle, 2013; Liu and Passaglia, 2011). In *M. sexta*, two biogenic amine-immunoreactive
702 neurons project into the sensory cell layer of the antenna, being suited to phase-shift endogenous
703 cAMP oscillations via stress signals such as octopamine (Flecke and Stengl, 2009; Schendzielorz et
704 al., 2015). Comparably, the circadian pacemaker center controls endogenous rhythms in the
705 electrical network activity in rodent brains via endogenous cAMP oscillations that are phase-
706 controlled through G-protein coupled receptor signaling (Ono et al., 2023; Prosser et al., 1989;
707 Prosser and Gillette, 1991). Future studies will explore the links between PTFL and TTFL clocks in
708 ORNs.

709 6.3 Circadian and ultradian rhythms in spontaneous ORN activity resemble the 710 physiologically relevant timescales for active sensing

711 Moths are more sensitive to pheromone stimulation during their activity phase than at rest,
712 apparently due to antennal circadian clocks (Flecke et al., 2010; Flecke and Stengl, 2009; Merlin et
713 al., 2007, 2006; Schendzielorz et al., 2015; Schuckel et al., 2007; Silvegren et al., 2005). The greater
714 the distance from the female, the lower the frequency of pheromone filaments in the air. The
715 increased pheromone sensitivity during the activity phase enhances the male's chance to detect

716 and locate a calling female. Pheromone concentration is encoded in the frequency of the first,
717 phasic burst of spikes of the characteristic triphasic spiking sequence of ORNs in response to brief
718 pheromone pulses, which is independent of Orco (Dolzer et al., 2003; Nolte et al., 2013; Schneider
719 et al., 2025). Consistent with these results, we found here that blocking Orco does not affect the
720 upper frequency band of spontaneous activity that correlates with the frequency ranges of the
721 pheromone-encoding primary fast pheromone response(Dolzer et al., 2003; Nolte et al., 2016,
722 2013). However, through the cAMP-dependent increase in Orco conductance during the activity
723 phase, the ORN membrane potential is closer to spike threshold and fewer pheromone molecules
724 are necessary to produce a receptor current that brings the membrane voltage over that threshold.
725 Thus, larger Orco conductance increases the likelihood of an ORN response to pheromone
726 stimulation without changing the typical triphasic spiking pattern of the response.
727 In the odor transduction of *Drosophila*, OR-Orco activation drives the initial receptor current
728 response (Sato et al., 2008; Wicher et al., 2008). In contrast, Orco is not part of an OR-Orco odor-
729 gated receptor ion channel complex in hawkmoths but controls the spontaneous ORN activity and
730 the late, long-lasting pheromone response (LLPR). The LLPR begins several hundred milliseconds
731 after the initiation of the pheromone-dependent transduction current and correlates with the time
732 course of pheromone-induced rises in cGMP levels, possibly playing a role in odor memory or long-
733 term gain control (Boekhoff et al., 1993; Nolte et al., 2016, 2013; Stengl, 2010; Stengl et al., 2001;
734 Wicher and Miazzi, 2021; Ziegelberger et al., 1990). Thus, in hawkmoths, Orco is not part of the
735 primary transduction channel but rather controls membrane potential oscillations and thereby the
736 temporal resolution and general pheromone sensitivity of ORNs. In addition, the increased
737 spontaneous burst frequency during the hawkmoth's activity phase improves the resolution of the
738 anticipated pheromone pulses during its mating flight in search for females.
739 In the mammalian suprachiasmatic nucleus (SCN), the clock that controls the sleep-wake
740 cycle, cAMP levels oscillate at an circadian frequency, and cAMP and cGMP induce ZT-dependent
741 opposing phase shifts in SCN spiking activity (Prosser et al., 1989; Prosser and Gillette, 1991). In
742 antennae of both *M. sexta* (Schendzielorz et al., 2015) and the cockroach *Rhyparobia maderae*
743 (Schendzielorz et al., 2012), cAMP levels express daily and circadian oscillations and peak during
744 the activity phase. In contrast, cGMP levels do not oscillate under constant conditions. They are in
745 antiphase to the daily oscillations in cAMP levels in LD and are elevated by strong or long
746 pheromone exposure, which adapts the sensitivity and temporal resolution of ORNs (Boekhoff et
747 al., 1993; Dolzer et al., 2021; Flecke et al., 2006; Schendzielorz et al., 2015; Ziegelberger et al.,

748 1990). This implies that cAMP and cGMP may have ZT-dependent effects on Orco conductivity,
749 thereby affecting pheromone sensitivity via control of the membrane potential and intracellular
750 Ca^{2+} concentrations.

751 The upregulation of neural activity during wakefulness/alertness seems to be ubiquitous
752 among different species. For example, the many synchronously recorded neurons in human EEG
753 show fast oscillations in the alpha, beta, and gamma frequency ranges during alertness and slow
754 oscillations in the delta and theta ranges during rest and sleep. Similarly, in the lower frequency
755 band, the spontaneous spiking activity of hawkmoth ORNs changes from below delta during rest to
756 theta/alpha ranges during their activity phase. The upper frequency band in the gamma range,
757 which did not depend on Orco regulation, comprises the spike frequency within a burst,
758 reminiscent of the first phasic pheromone response that encodes pheromone concentration
759 changes (Dolzer et al., 2003). The increased spontaneous spiking activity in the theta/alpha range
760 during the activity phase of the hawkmoth matches the maximal temporal resolution of pheromone
761 pulses of up to 10 Hz (Marion-Poll and Tobin, 1992), which supports a role for Orco as part of a
762 membrane-bound PTFL clockwork that tunes the ORNs for active sensing. Even through
763 oscillations in the field potential of electroantennogram responses to odor stimulation can reach
764 100 Hz in different insects (Szyszka et al., 2014), these frequencies most likely do not encode the
765 temporal resolution of physiological odor responses. Apparently, they reflect the astounding
766 adaptive ability of antennal ORNs to synchronize their endogenous membrane potential
767 oscillations across the antenna to a broad range of stimulation frequencies. Pheromone pulse
768 resolution of about 100 Hz was never reported in single olfactory sensilla recordings, and in
769 behavioral experiments male moths stopped their upwind mate search if pheromone pulses
770 exceeded 30 Hz, apparently due to adaptation (Baker et al., 1985; Bau et al., 2005, 2002; Tripathy et
771 al., 2010).

772 Circadian oscillations in the ORN membrane potential would be ideally suited to tune
773 sensitivity and temporal resolution of the pheromone-sensitive ORNs to the hawkmoth's rest-
774 activity cycle, synchronizing male and female mating behavior. Here, we have demonstrated how
775 modulation of a leaky pacemaker channel can achieve these circadian oscillations. Whether cAMP
776 levels are under control of the TTFL clock or oscillate based on Ca^{2+} concentration oscillations, and
777 would therefore be part of a stand-alone PTFL clock, remains to be studied.

6.4 Stochastic ion channel dynamics and circadian modulation of Orco conductance explain modeled ORN firing patterns

Our modeling results provide mechanistic insight into the irregular spontaneous activity of pheromone-sensitive ORNs in *M. sexta*, highlighting how stochastic ion channel dynamics and circadian modulation of ion conductance together shape spiking patterns. By employing a Langevin approximation of the stochastic HH formalism, we demonstrate that the intrinsic noise arising from the random gating of ion channels is sufficient to generate both isolated spikes and bursts of spikes, as observed experimentally. Our model effectively recapitulates the spike distributions found *in vivo* and accounts for the role of channel noise as a critical determinant of ORN firing patterns.

A key contribution of our model is the incorporation of the Orco ion channel as a pacemaker component, with a conductance that varies linearly with cAMP concentration. We show that circadian modulation of Orco conductance alone is sufficient to produce the observed time-of-day dependent changes in spike distribution. This finding suggests that the rhythmic expression of cAMP levels across the circadian cycle may act as a primary driver of diurnal changes in ORN excitability, without requiring additional external inputs or modulation of other ion channels.

Importantly, our results reveal that the same set of ion channels can support the emergence of both single action potentials and complex bursting behaviors purely through the stochastic variability of their gating kinetics. This unifying explanation reduces the need for invoking separate biophysical mechanisms or circuit-level inputs to explain these distinct firing modes.

For simplicity, the circadian variation in cAMP concentration was modeled using a sinusoidal function. While this approximation is sufficient for capturing the qualitative features of the rhythmic modulation, future work could enhance the biological realism of the model by coupling Orco conductance dynamics to a molecular circadian oscillator, such as a Goodwin-type TTFL. Incorporating this layer would allow for a more detailed exploration of how molecular clock components regulate cAMP synthesis and degradation. Additionally, further extensions could include downstream regulatory mechanisms such as phosphorylation and dephosphorylation events mediated by kinases and phosphatases under circadian control, potentially contributing to fine-tuned modulation of ion channel function over the daily cycle.

Together, these findings demonstrate the value of a biophysically grounded, noise-inclusive modeling framework for understanding complex temporal patterns in sensory neuron activity and

open the door for future integrative models linking molecular circadian clocks to cellular excitability.

7 References

Bahk S, Jones WD. 2016. Insect odorant receptor trafficking requires calmodulin. BMC Biology **14**:83. DOI: https://doi.org/10.1186/s12915-016-0306-x

Baker TC, Vogt RG. 1988. Measured Behavioural Latency in Response to Sex-Pheromone Loss in the Large Silk Moth *Antheraea Polyphemus*. Journal of Experimental Biology **137**:29–38. DOI: https://doi.org/10.1242/jeb.137.1.29

Baker TC, Willis MA, Haynes KF, Phelan PL. 1985. A pulsed cloud of sex pheromone elicits upwind flight in male moths. Physiological Entomology **10**:257–265. DOI: https://doi.org/10.1111/j.1365-3032.1985.tb00045.x

Battelle B-A. 2013. What the Clock Tells the Eye: Lessons from an Ancient Arthropod. Integrative and Comparative Biology **53**:144–153. DOI: https://doi.org/10.1093/icb/ict020, PMID: 23639718

Bau J, Justus KA, Cardé RT. 2002. Antennal resolution of pulsed pheromone plumes in three moth species. Journal of Insect Physiology **48**:433–442. DOI: https://doi.org/10.1016/S0022-1910(02)00062-8

Bau J, Justus KA, Loudon C, Cardé RT. 2005. Electroantennographic Resolution of Pulsed Pheromone Plumes in Two Species of Moths with Bipectinate Antennae. Chemical Senses **30**:771–780. DOI: https://doi.org/10.1093/chemse/bji069

Bell RA, Joachim FG. 1976. Techniques for Rearing Laboratory Colonies of Tobacco Hornworms and Pink Bollworms1. Annals of the Entomological Society of America **69**:365–373. DOI: https://doi.org/10.1093/aesa/69.2.365

Benton R, Sachse S, Michnick SW, Vosshall LB. 2006. Atypical Membrane Topology and Heteromeric Function of Drosophila Odorant Receptors In Vivo. PLOS Biology **4**:e20. DOI: https://doi.org/10.1371/journal.pbio.0040020

Boekhoff I, Seifert E, Göggerle S, Lindemann M, Krüger B-W, Breer H. 1993. Pheromone-induced second-messenger signaling in insect antennae. Insect Biochemistry and Molecular Biology **23**:757–762. DOI: https://doi.org/10.1016/0965-1748(93)90063-X

Bose A, Golowasch J, Guan Y, Nadim F. 2014. The role of linear and voltage-dependent ionic currents in the generation of slow wave oscillations. Journal of Computational Neuroscience **37**:229–242. DOI: https://doi.org/10.1007/s10827-014-0498-4

Butterwick JA, del Mármol J, Kim KH, Kahlson MA, Rogow JA, Walz T, Ruta V. 2018. Cryo-EM structure of the insect olfactory receptor Orco. Nature **560**:447–452. DOI: https://doi.org/10.1038/s41586-018-0420-8

Cao L-H, Jing B-Y, Yang D, Zeng X, Shen Y, Tu Y, Luo D-G. 2016. Distinct signaling of *Drosophila* chemoreceptors in olfactory sensory neurons. Proceedings of the National Academy of Sciences **113**:E902–E911. DOI: https://doi.org/10.1073/pnas.1518329113

Chen S, Luetje CW. 2012. Identification of New Agonists and Antagonists of the Insect Odorant Receptor Co-Receptor Subunit. PLOS ONE **7**:e36784. DOI: https://doi.org/10.1371/journal.pone.0036784

Cochet-Bissuel M, Lory P, Monteil A. 2014. The sodium leak channel, NALCN, in health and disease. Frontiers in Cellular Neuroscience **8**:132. DOI: https://doi.org/10.3389/fncel.2014.00132, PMID: 24904279

Dacks AM, Dacks JB, Christensen TA, Nighorn AJ. 2006. The cloning of one putative octopamine receptor and two putative serotonin receptors from the tobacco hawkmoth, *Manduca sexta*. Insect Biochemistry and Molecular Biology **36**:741–747. DOI: https://doi.org/10.1016/j.ibmb.2006.07.002

Das A, Holmes TC, Sheeba V. 2016. dTRPA1 in Non-circadian Neurons Modulates Temperature-dependent Rhythmic Activity in *Drosophila melanogaster*. Journal of Biological Rhythms **31**:272–288. DOI: https://doi.org/10.1177/0748730415627037

Dolzer J, Fischer K, Stengl M. 2003. Adaptation in pheromone-sensitive trichoid sensilla of the hawkmoth *Manduca sexta*. Journal of Experimental Biology **206**:1575–1588. DOI: https://doi.org/10.1242/jeb.00302

Dolzer J, Krannich S, Fischer K, Stengl M. 2001. Oscillations of the Transepithelial Potential of Moth Olfactory Sensilla Are Influenced by Octopamine and Serotonin. Journal of Experimental Biology **204**:2781–2794. DOI: https://doi.org/10.1242/jeb.204.16.2781

Dolzer J, Krannich S, Stengl M. 2008. Pharmacological Investigation of Protein Kinase C- and cGMP-Dependent Ion Channels in Cultured Olfactory Receptor Neurons of the Hawkmoth *Manduca sexta*. Chemical Senses **33**:803–813. DOI: https://doi.org/10.1093/chemse/bjn043

Dolzer J, Schröder K, Stengl M. 2021. Cyclic nucleotide-dependent ionic currents in olfactory receptor neurons of the hawkmoth *Manduca sexta* suggest pull–push sensitivity modulation. European Journal of Neuroscience **54**:4804–4826. DOI: https://doi.org/10.1111/ejn.15346

Dubowy C, Sehgal A. 2017. Circadian Rhythms and Sleep in *Drosophila melanogaster*. Genetics **205**:1373–1397. DOI: https://doi.org/10.1534/genetics.115.185157

Edgar RS, Green EW, Zhao Y, van Ooijen G, Olmedo M, Qin X, Xu Y, Pan M, Valekunja UK, Feeney KA, Maywood ES, Hastings MH, Baliga NS, Merrow M, Millar AJ, Johnson CH, Kyriacou CP, O'Neill JS, Reddy AB. 2012. Peroxiredoxins are conserved markers of circadian rhythms. Nature **485**:459–464. DOI: https://doi.org/10.1038/nature11088, PMID: 22622569

Fandino RA, Haverkamp A, Bisch-Knaden S, Zhang J, Bucks S, Nguyen TAT, Schröder K, Werckenthin A, Rybak J, Stengl M, Knaden M, Hansson BS, Große-Wilde E. 2019. Mutagenesis of odorant coreceptor Orco fully disrupts foraging but not oviposition behaviors in the hawkmoth *Manduca sexta*. Proceedings of the National Academy of Sciences **116**:15677–15685. DOI: https://doi.org/10.1073/pnas.1902089116

Flecke C, Dolzer J, Krannich S, Stengl M. 2006. Perfusion with cGMP analogue adapts the action potential response of pheromone-sensitive sensilla trichoidea of the hawkmoth *Manduca sexta* in a daytime-dependent manner. Journal of Experimental Biology **209**:3898–3912. DOI: https://doi.org/10.1242/jeb.02432

Flecke C, Nolte A, Stengl M. 2010. Perfusion with cAMP analogue affects pheromone-sensitive trichoid sensilla of the hawkmoth *Manduca sexta* in a time-dependent manner. Journal of Experimental Biology **213**:842–852. DOI: https://doi.org/10.1242/jeb.032839

Flecke C, Stengl M. 2009. Octopamine and tyramine modulate pheromone-sensitive olfactory sensilla of the hawkmoth *Manduca sexta* in a time-dependent manner. Journal of Comparative Physiology A **195**:529–545. DOI: https://doi.org/10.1007/s00359-009-0429-4

Forlino M, Vijayan A, Schneider AC, Stengl M, Garcia ME. 2025. ORN-Orco-Model. https://github.com/a-c-schneider/VijayanForlinoEtAl2025_Model

Fox RF, Lu Y. 1994. Emergent collective behavior in large numbers of globally coupled independently stochastic ion channels. Physical Review E **49**:3421–3431. DOI: https://doi.org/10.1103/PhysRevE.49.3421

Gawalek P, Stengl M. 2018. The Diacylglycerol Analogs OAG and DOG Differentially Affect Primary Events of Pheromone Transduction in the Hawkmoth *Manduca sexta* in a Zeitgebertime-Dependent Manner Apparently Targeting TRP Channels. Frontiers in Cellular Neuroscience **12**:218. DOI: https://doi.org/10.3389/fncel.2018.00218

Géron A, Werner ,Johannes, Wattiez ,Ruddy, and Matallana-Surget S. 2024. Towards the discovery of novel molecular clocks in Prokaryotes. Critical Reviews in Microbiology **50**:491–503. DOI: https://doi.org/10.1080/1040841X.2023.2220789, PMID: 37330701

Getahun MN, Olsson SB, Lavista-Llanos S, Hansson BS, Wicher D. 2013. Insect Odorant Response Sensitivity Is Tuned by Metabotropically Autoregulated Olfactory Receptors. PLOS ONE **8**:e58889. DOI: https://doi.org/10.1371/journal.pone.0058889

Getahun MN, Thoma M, Lavista-Llanos S, Keesey I, Fandino RA, Knaden M, Wicher D, Olsson SB, Hansson BS. 2016. Intracellular regulation of the insect chemoreceptor complex impacts odour localization in flying insects. Journal of Experimental Biology **219**:3428–3438. DOI: https://doi.org/10.1242/jeb.143396

Ghosh S, Suray C, Bozzolan F, Palazzo A, Monsempès C, Lecouvreur F, Chatterjee A. 2024. Pheromone-mediated command from the female to male clock induces and synchronizes circadian rhythms of the moth *Spodoptera littoralis*. Current biology **34**:1414-1425.e5. DOI: https://doi.org/10.1016/j.cub.2024.02.042, PMID: 38479388

Goldstein SAN, Bockenhauer D, O'Kelly I, Zilberberg N. 2001. Potassium leak channels and the KCNK family of two-p-domain subunits. Nature Reviews Neuroscience **2**:175–184. DOI: https://doi.org/10.1038/35058574

Golowasch J, Bose A, Guan Y, Salloum D, Roeser A, Nadim F. 2017. A balance of outward and linear inward ionic currents is required for generation of slow-wave oscillations. Journal of Neurophysiology **118**:1092–1104. DOI: https://doi.org/10.1152/jn.00240.2017

Guo H, Smith DP. 2022. Time-Dependent Odorant Sensitivity Modulation in Insects. Insects **13**:354. DOI: https://doi.org/10.3390/insects13040354

Guo H, Smith DP. 2017. Odorant Receptor Desensitization in Insects. Journal of Experimental Neuroscience **11**:1179069517748600. DOI: https://doi.org/10.1177/1179069517748600

Hall JC, Rosbash M. 1993. Oscillating molecules and how they move circadian clocks across evolutionary boundaries. Proceedings of the National Academy of Sciences of the United States of America **90**:5382–5383. PMID: 8516281

Halls ML, Cooper DMF. 2011. Regulation by Ca2+-Signaling Pathways of Adenylyl Cyclases. Cold Spring Harbor Perspectives in Biology **3**:a004143. DOI: https://doi.org/10.1101/cshperspect.a004143, PMID: 21123395

Hardin PE. 2011. Molecular Genetic Analysis of Circadian Timekeeping in *Drosophila*. In: Brody S (Ed). *Advances in Genetics*, The Genetics of Circadian Rhythms. Academic Press. p. 141–173. DOI: https://doi.org/10.1016/B978-0-12-387690-4.00005-2

Hastings MH, Smyllie NJ, Patton AP. 2020. Molecular-genetic Manipulation of the Suprachiasmatic Nucleus Circadian Clock. Journal of Molecular Biology **432**:3639–3660. DOI: https://doi.org/10.1016/j.jmb.2020.01.019, PMID: 31996314

Hille B. 2001. Ion Channels of Excitable Membranes, Third Edition, Third Edition. Oxford University Press.

Itagaki H, Conner WE. 1988. Calling Behavior of *Manduca sexta* (L.) (Lepidoptera: Sphingidae) with Notes on the Morphology of the Female Sex Pheromone Gland. Annals of the Entomological Society of America **81**:798–807. DOI: https://doi.org/10.1093/aesa/81.5.798

Jain K, Lavista-Llanos S, Grabe V, Hansson BS, Wicher D. 2021. Calmodulin regulates the olfactory performance in Drosophila melanogaster. Scientific Reports **11**:3747. DOI: https://doi.org/10.1038/s41598-021-83296-9

Jones PL, Pask GM, Rinker DC, Zwiebel LJ. 2011. Functional agonism of insect odorant receptor ion channels. Proceedings of the National Academy of Sciences **108**:8821–8825. DOI: https://doi.org/10.1073/pnas.1102425108

Kaissling KE, Hildebrand JG, Tumlinson JH. 1989. Pheromone receptor cells in the male moth *Manduca sexta*. Archives of Insect Biochemistry and Physiology **10**:273–279. DOI: https://doi.org/10.1002/arch.940100403

Kaissling KE, Thorson J. 1980. Insect Olfactory Sensilla: Structural, Chemical and Electrical Aspects of the Functional Organisation. In: Sattelle DB, Hall LM, Hildebrand JG (Eds). *Receptors for Neurotransmitters, Hormones and Pheromones in Insects*. Elsevier/North-Holland Biomedical Press. p. 261–282.

Kaissling KE, Zack Strausfeld C, Rumbo ER. 1987. Adaptation processes in insect olfactory receptors. Mechanisms and behavioral significance. Annals of the New York Academy of Sciences **510**:104–112. DOI: https://doi.org/10.1111/j.1749-6632.1987.tb43475.x, PMID: 3324874

Kalinová B, Hoskovec M, Liblikas I, Unelius CR, Hansson BS. 2001. Detection of Sex Pheromone Components in *Manduca sexta* (L.). Chemical Senses **26**:1175–1186. DOI: https://doi.org/10.1093/chemse/26.9.1175

Kodirov SA. 2022. Probability that there is a mammalian counterpart of cardiac clock in insects. Archives of Insect Biochemistry and Physiology **110**:e21867. DOI: https://doi.org/10.1002/arch.21867

Krishnan B, Dryer SE, Hardin PE. 1999. Circadian rhythms in olfactory responses of *Drosophila melanogaster*. Nature **400**:375–378. DOI: https://doi.org/10.1038/22566

Lamont EW, Amir S. 2010. Circadian and Ultradian Clocks/Rhythms. In: Koob GF, Moal ML, Thompson RF (Eds). *Encyclopedia of Behavioral Neuroscience*. Academic Press. p. 257–261. DOI: https://doi.org/10.1016/B978-0-08-045396-5.00223-2

Lee C-H, MacKinnon R. 2017. Structures of the Human HCN1 Hyperpolarization-Activated Channel. Cell **168**:111-120.e11. DOI: https://doi.org/10.1016/j.cell.2016.12.023

Lee JK, Strausfeld NJ. 1990. Structure, distribution and number of surface sensilla and their receptor cells on the olfactory appendage of the male mothManduca sexta. Journal of Neurocytology **19**:519–538. DOI: https://doi.org/10.1007/BF01257241

Liu JS, Passaglia CL. 2011. Spike firing pattern of output neurons of the Limulus circadian clock. Journal of Biological Rhythms **26**:335–344. DOI: https://doi.org/10.1177/0748730411409712, PMID: 21775292

Livak KJ, Schmittgen TD. 2001. Analysis of relative gene expression data using real-time quantitative PCR and the $2^{-\Delta\Delta C(T)}$ Method. Methods (San Diego, Calif.) **25**:402–408. DOI: https://doi.org/10.1006/meth.2001.1262, PMID: 11846609

Lüthi A, McCormick DA. 1998. H-Current: Properties of a Neuronal and Network Pacemaker. Neuron **21**:9–12. DOI: https://doi.org/10.1016/S0896-6273(00)80509-7

Mandala VS, Fu Z, MacKinnon R. 2025. Molecular contacts in self-assembling clusters of membrane proteins. Proceedings of the National Academy of Sciences **122**:e2507112122. DOI: https://doi.org/10.1073/pnas.2507112122

Marion-Poll F, Tobin TR. 1992. Temporal coding of pheromone pulses and trains in *Manduca sexta*. Journal of Comparative Physiology A **171**:505–512. DOI: https://doi.org/10.1007/BF00194583

Martín F, Charro M, Alcorta E. 2001. Mutations affecting the cAMP transduction pathway modify olfaction in *Drosophila*. Journal of Comparative Physiology A **187**:359–370. DOI: https://doi.org/10.1007/s003590100208

Merlin C, François M-C, Queguiner I, Maïbèche-Coisné M, Jacquin-Joly E. 2006. Evidence for a putative antennal clock in *Mamestra brassicae*: Molecular cloning and characterization of two clock genes –*period* and *cryptochrome*– in antennae. Insect Molecular Biology **15**:137–145. DOI: https://doi.org/10.1111/j.1365-2583.2006.00617.x

Merlin C, Gegear RJ, Reppert SM. 2009. Antennal Circadian Clocks Coordinate Sun Compass Orientation in Migratory Monarch Butterflies. Science **325**:1700–1704. DOI: https://doi.org/10.1126/science.1176221

Merlin C, Lucas P, Rochat D, François M-C, Maïbèche-Coisne M, Jacquin-Joly E. 2007. An Antennal Circadian Clock and Circadian Rhythms in Peripheral Pheromone Reception in the Moth *Spodoptera littoralis*. Journal of Biological Rhythms **22**:502–514. DOI: https://doi.org/10.1177/0748730407307737

Millar AJ. 2016. The Intracellular Dynamics of Circadian Clocks Reach for the Light of Ecology and Evolution. Annual Review of Plant Biology **67**:595–618. DOI: https://doi.org/10.1146/annurev-arplant-043014-115619

Mönke G, Sorgenfrei FA, Schmal C, Granada AE. 2020. Optimal time frequency analysis for biological data - pyBOAT. DOI: https://doi.org/10.1101/2020.04.29.067744

Mukunda L, Miazzi F, Kaltofen S, Hansson BS, Wicher D. 2014. Calmodulin modulates insect odorant receptor function. Cell Calcium **55**:191–199. DOI: https://doi.org/10.1016/j.ceca.2014.02.013

Mukunda L, Miazzi F, Sargsyan V, Hansson BS, Wicher D. 2016. Calmodulin Affects Sensitization of *Drosophila melanogaster* Odorant Receptors. Frontiers in Cellular Neuroscience **10**. DOI: https://doi.org/10.3389/fncel.2016.00028

Nakagawa T, Vosshall LB. 2009. Controversy and consensus: noncanonical signaling mechanisms in the insect olfactory system. Current Opinion in Neurobiology **19**:284–292. DOI: https://doi.org/10.1016/j.conb.2009.07.015

Nishiitsutsuji-Uwo J, Pittendrigh CS. 1968. Central nervous system control of circadian rhythmicity in the cockroach II. The pathway of light signals that entrain the rhythm. Zeitschrift für vergleichende Physiologie **58**:1–13. DOI: https://doi.org/10.1007/BF00302433

Nolte A, Funk NW, Mukunda L, Gawalek P, Werckenthin A, Hansson BS, Wicher D, Stengl M. 2013. In situ Tip-Recordings Found No Evidence for an Orco-Based Ionotropic Mechanism of Pheromone-Transduction in *Manduca sexta*. PLOS ONE **8**:e62648. DOI: https://doi.org/10.1371/journal.pone.0062648

Nolte A, Gawalek P, Koerte S, Wei H, Schumann R, Werckenthin A, Krieger J, Stengl M. 2016. No Evidence for Ionotropic Pheromone Transduction in the Hawkmoth *Manduca sexta*. PLOS ONE **11**:e0166060. DOI: https://doi.org/10.1371/journal.pone.0166060

O'Neill JS, Reddy AB. 2011. Circadian clocks in human red blood cells. Nature **469**:498–503. DOI: https://doi.org/10.1038/nature09702

Ono D, Wang Huan, Hung CJ, Wang Hsin-tzu, Kon N, Yamanaka A, Li Y, Sugiyama T. 2023. Network-driven intracellular cAMP coordinates circadian rhythm in the suprachiasmatic nucleus. Science Advances **9**:eabq7032. DOI: https://doi.org/10.1126/sciadv.abq7032

Page TL, Koelling E. 2003. Circadian rhythm in olfactory response in the antennae controlled by the optic lobe in the cockroach. Journal of Insect Physiology **49**:697–707. DOI: https://doi.org/10.1016/s0022-1910(03)00071-4, PMID: 12837322

Pask GM, Bobkov YV, Corey EA, Ache BW, Zwiebel LJ. 2013. Blockade of Insect Odorant Receptor Currents by Amiloride Derivatives. Chemical Senses **38**:221–229. DOI: https://doi.org/10.1093/chemse/bjs100

Patel AJ, Honoré E. 2001. Properties and modulation of mammalian 2P domain K+ channels. Trends in Neurosciences **24**:339–346. DOI: https://doi.org/10.1016/S0166-2236(00)01810-5

Pézier A, Acquistapace A, Renou M, Rospars J-P, Lucas P. 2007. Ca^{2+} Stabilizes the Membrane Potential of Moth Olfactory Receptor Neurons at Rest and Is Essential for Their Fast Repolarization. Chemical Senses **32**:305–317. DOI: https://doi.org/10.1093/chemse/bjl059

1047 Plautz JD, Kaneko M, Hall JC, Kay SA. 1997. Independent Photoreceptive Circadian Clocks
1048 Throughout *Drosophila*. Science **278**:1632–1635. DOI:
1049 https://doi.org/10.1126/science.278.5343.1632
1050 Prosser RA, Gillette MU. 1991. Cyclic changes in cAMP concentration and phosphodiesterase
1051 activity in a mammalian circadian clock studied *in vitro*. Brain Research **568**:185–192. DOI:
1052 https://doi.org/10.1016/0006-8993(91)91396-I
1053 Prosser RA, McArthur AJ, Gillette MU. 1989. cGMP induces phase shifts of a mammalian circadian
1054 pacemaker at night, in antiphase to cAMP effects. Proceedings of the National Academy of
1055 Sciences of the United States of America **86**:6812–6815. PMID: 2549549
1056 Pu S, Thomas PJ. 2020. Fast and Accurate Langevin Simulations of Stochastic Hodgkin-Huxley
1057 Dynamics. Neural Computation **32**:1775–1835. DOI:
1058 https://doi.org/10.1162/neco_a_01312
1059 Ratliff J, Franci A, Marder E, O'Leary T. 2021. Neuronal oscillator robustness to multiple global
1060 perturbations. Biophysical Journal **120**:1454–1468. DOI:
1061 https://doi.org/10.1016/j.bpj.2021.01.038
1062 Redkozubov A. 2000. Guanosine 3',5'-Cyclic Monophosphate Reduces the Response of the Moth's
1063 Olfactory Receptor Neuron to Pheromone. Chemical Senses **25**:381–385. DOI:
1064 https://doi.org/10.1093/chemse/25.4.381
1065 Reinhard N, Fukuda A, Manoli G, Derksen E, Saito A, Möller G, Sekiguchi M, Rieger D, Helfrich-
1066 Förster C, Yoshii T, Zandawala M. 2024. Synaptic connectome of the *Drosophila* circadian
1067 clock. Nature Communications **15**:10392. DOI: https://doi.org/10.1038/s41467-024-54694-
1068 0
1069 Riffell JA, Abrell L, Hildebrand JG. 2008. Physical processes and real-time chemical measurement
1070 of the insect olfactory environment. Journal of Chemical Ecology **34**:837–853. DOI:
1071 https://doi.org/10.1007/s10886-008-9490-7, PMID: 18548311
1072 Robinson RB, Siegelbaum SA. 2003. Hyperpolarization-activated cation currents: from molecules
1073 to physiological function. Annual Review of Physiology **65**:453–480. DOI:
1074 https://doi.org/10.1146/annurev.physiol.65.092101.142734, PMID: 12471170
1075 Sargsyan V, Getahun MN, Lavista Llanos S, Olsson SB, Hansson BS, Wicher D. 2011.
1076 Phosphorylation via PKC Regulates the Function of the *Drosophila* Odorant Co-Receptor.
1077 Frontiers in Cellular Neuroscience **5**. DOI: https://doi.org/10.3389/fncel.2011.00005
1078 Sato K, Pellegrino M, Nakagawa Takao, Nakagawa Tatsuro, Vosshall LB, Touhara K. 2008. Insect
1079 olfactory receptors are heteromeric ligand-gated ion channels. Nature **452**:1002–1006.
1080 DOI: https://doi.org/10.1038/nature06850
1081 Sauman I, Reppert SM. 1998. Brain Control of Embryonic Circadian Rhythms in the Silkmoth
1082 *Antheraea pernyi*. Neuron **20**:741–748. DOI: https://doi.org/10.1016/S0896-6273(00)81012-
1083 0
1084 Schendzielorz J, Schendzielorz T, Arendt A, Stengl M. 2014. Bimodal Oscillations of Cyclic
1085 Nucleotide Concentrations in the Circadian System of the Madeira Cockroach *Rhyparobia*
1086 *maderae*. Journal of Biological Rhythms **29**:318–331. DOI:
1087 https://doi.org/10.1177/0748730414546133
1088 Schendzielorz T, Peters W, Boekhoff I, Stengl M. 2012. Time of Day Changes in Cyclic Nucleotides
1089 Are Modified via Octopamine and Pheromone in Antennae of the Madeira Cockroach.
1090 Journal of Biological Rhythms **27**:388–397. DOI:
1091 https://doi.org/10.1177/0748730412456265
1092 Schendzielorz T, Schirmer K, Stolte P, Stengl M. 2015. Octopamine Regulates Antennal Sensory
1093 Neurons via Daytime-Dependent Changes in cAMP and IP_3 Levels in the Hawkmoth

Manduca sexta. PLOS ONE **10**:e0121230. DOI: https://doi.org/10.1371/journal.pone.0121230

Schmidt DR, Galán RF, Thomas PJ. 2018. Stochastic shielding and edge importance for Markov chains with timescale separation. PLOS Computational Biology **14**:e1006206. DOI: https://doi.org/10.1371/journal.pcbi.1006206

Schmidt DR, Thomas PJ. 2014. Measuring Edge Importance: A Quantitative Analysis of the Stochastic Shielding Approximation for Random Processes on Graphs. The Journal of Mathematical Neuroscience **4**:6. DOI: https://doi.org/10.1186/2190-8567-4-6

Schneider AC, Schröder K, Chang Y, Nolte A, Gawalek P, Stengl M. 2025. Hawkmoth Pheromone Transduction Involves G-Protein–Dependent Phospholipase Cβ Signaling. eNeuro **12**:ENEURO.0376-24.2024. DOI: https://doi.org/10.1523/ENEURO.0376-24.2024, PMID: 39880675

Schuckel J, Siwicki KK, Stengl M. 2007. Putative circadian pacemaker cells in the antenna of the hawkmoth *Manduca sexta*. Cell and Tissue Research **330**:271–278. DOI: https://doi.org/10.1007/s00441-007-0471-x

Schweitzer ES, Sanes JR, Hildebrand JG. 1976. Ontogeny of electroantennogram responses in the moth, *Manduca sexta*. Journal of Insect Physiology **22**:955–960. DOI: https://doi.org/10.1016/0022-1910(76)90078-0

Sharma A, Rahman G, Gorelik J, Bhargava A. 2023. Voltage-Gated T-Type Calcium Channel Modulation by Kinases and Phosphatases: The Old Ones, the New Ones, and the Missing Ones. Cells **12**:461. DOI: https://doi.org/10.3390/cells12030461, PMID: 36766802

Silvegren G, Löfstedt C, Qi Rosén W. 2005. Circadian mating activity and effect of pheromone pre-exposure on pheromone response rhythms in the moth *Spodoptera littoralis*. Journal of Insect Physiology **51**:277–286. DOI: https://doi.org/10.1016/j.jinsphys.2004.11.013

Steinbrecht RA. 1992. Experimental morphology of insect olfaction: Tracer studies, x-ray microanalysis, autoradiography, and immunocytochemistry with silkmoth antennae. Microscopy Research and Technique **22**:336–350. DOI: https://doi.org/10.1002/jemt.1070220404

Stengl M. 2010. Pheromone Transduction in Moths. Frontiers in Cellular Neuroscience **4**:133. DOI: https://doi.org/10.3389/fncel.2010.00133

Stengl M. 1994. Inositol-trisphosphate-dependent calcium currents precede cation currents in insect olfactory receptor neurons *in vitro*. Journal of Comparative Physiology A **174**:187–194. DOI: https://doi.org/10.1007/BF00193785

Stengl M. 1993. Intracellular-Messenger-Mediated Cation Channels in Cultured Olfactory Receptor Neurons. Journal of Experimental Biology **178**:125–147. DOI: https://doi.org/10.1242/jeb.178.1.125

Stengl M, Funk NW. 2013. The role of the coreceptor Orco in insect olfactory transduction. Journal of Comparative Physiology A **199**:897–909. DOI: https://doi.org/10.1007/s00359-013-0837-3

Stengl M, Schneider AC. 2024. Contribution of membrane-associated oscillators to biological timing at different timescales. Frontiers in Physiology **14**:1243455. DOI: https://doi.org/10.3389/fphys.2023.1243455

Stengl M, Schröder K. 2021. 14 - Multiscale timing of pheromone transduction in hawkmoth olfactory receptor neurons. In: Blomquist GJ, Vogt RG (Eds). *Insect Pheromone Biochemistry and Molecular Biology (Second Edition)*. Academic Press. p. 435–468. DOI: https://doi.org/10.1016/B978-0-12-819628-1.00014-6

1140 Stengl M, Zintl R, De Vente J, Nighorn A. 2001. Localization of cGMP immunoreactivity and of
1141 soluble guanylyl cyclase in antennal sensilla of the hawkmoth Manduca sexta. Cell and
1142 Tissue Research **304**:409–421. DOI: https://doi.org/10.1007/s004410000336
1143 Szyszka P, Gerkin RC, Galizia CG, Smith BH. 2014. High-speed odor transduction and pulse
1144 tracking by insect olfactory receptor neurons. Proceedings of the National Academy of
1145 Sciences **111**:16925–16930. DOI: https://doi.org/10.1073/pnas.1412051111
1146 Talley EM, Solórzano G, Lei Q, Kim D, Bayliss DA. 2001. CNS Distribution of Members of the Two-
1147 Pore-Domain (KCNK) Potassium Channel Family. Journal of Neuroscience **21**:7491–7505.
1148 DOI: https://doi.org/10.1523/JNEUROSCI.21-19-07491.2001, PMID: 11567039
1149 Tanoue S, Krishnan P, Krishnan B, Dryer SE, Hardin PE. 2004. Circadian Clocks in Antennal
1150 Neurons Are Necessary and Sufficient for Olfaction Rhythms in *Drosophila*. Current Biology
1151 **14**:638–649. DOI: https://doi.org/10.1016/j.cub.2004.04.009, PMID: 15084278
1152 Thaben PF, Westermark PO. 2014. Detecting Rhythms in Time Series with RAIN. Journal of
1153 Biological Rhythms **29**:391–400. DOI: https://doi.org/10.1177/0748730414553029
1154 Thaiss CA, Zeevi D, Levy M, Zilberman-Schapira G, Suez J, Tengeler AC, Abramson L, Katz MN,
1155 Korem T, Zmora N, Kuperman Y, Biton I, Gilad S, Harmelin A, Shapiro H, Halpern Z, Segal E,
1156 Elinav E. 2014. Transkingdom Control of Microbiota Diurnal Oscillations Promotes
1157 Metabolic Homeostasis. Cell **159**:514–529. DOI: https://doi.org/10.1016/j.cell.2014.09.048
1158 Tripathy S, Staudacher EM, Peters O, Kalwar F, Hatfield M, Daly K. 2010. Odors pulsed at wing beat
1159 frequencies are tracked by primary olfactory networks and enhance odor detection.
1160 Frontiers in Cellular Neuroscience **4**. DOI: https://doi.org/10.3389/neuro.03.001.2010
1161 Viertel R, Borisyuk A. 2019. A Computational model of the mammalian external tufted cell. Journal
1162 of Theoretical Biology **462**:109–121. DOI: https://doi.org/10.1016/j.jtbi.2018.10.003
1163 Wicher D. 2018. Tuning Insect Odorant Receptors. Frontiers in Cellular Neuroscience **12**:94. DOI:
1164 https://doi.org/10.3389/fncel.2018.00094, PMID: 29674957
1165 Wicher D, Miazzi F. 2021. Functional properties of insect olfactory receptors: ionotropic receptors
1166 and odorant receptors. Cell and Tissue Research **383**:7–19. DOI:
1167 https://doi.org/10.1007/s00441-020-03363-x
1168 Wicher D, Schäfer R, Bauernfeind R, Stensmyr MC, Heller R, Heinemann SH, Hansson BS. 2008.
1169 *Drosophila* odorant receptors are both ligand-gated and cyclic-nucleotide-activated cation
1170 channels. Nature **452**:1007–1011. DOI: https://doi.org/10.1038/nature06861
1171 Zhou X, Yuan C, Guo A. 2005. *Drosophila* Olfactory Response Rhythms Require Clock Genes but
1172 Not Pigment Dispersing Factor or Lateral Neurons. Journal of Biological Rhythms **20**:237–
1173 244. DOI: https://doi.org/10.1177/0748730405274451
1174 Ziegelberger G, Berg M van den, Kaissling KE, Klumpp S, Schultz JE. 1990. Cyclic GMP levels and
1175 guanylate cyclase activity in pheromone-sensitive antennae of the silkmoths *Antheraea*
1176 *polyphemus* and *Bombyx mori*. Journal of Neuroscience **10**:1217–1225. DOI:
1177 https://doi.org/10.1523/JNEUROSCI.10-04-01217.1990, PMID: 1970356
1178

8 Figures and Figure legends

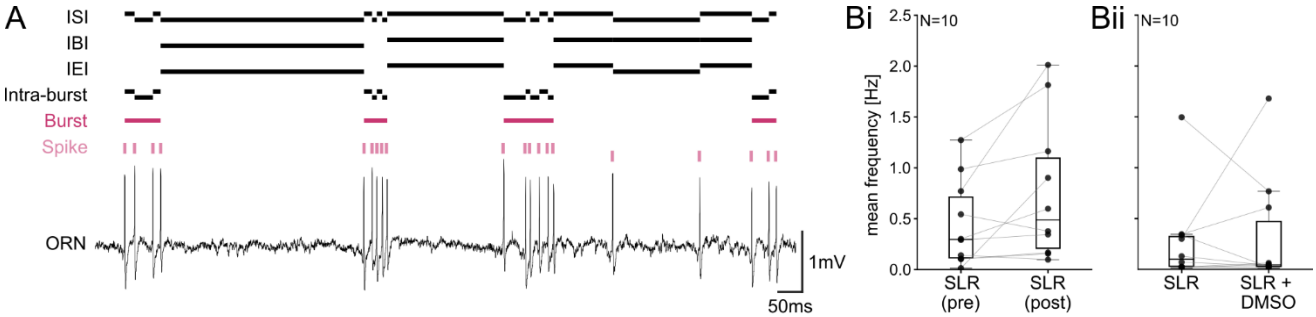

Figure 1: Attributes of pheromone-sensitive ORN spiking patterns.

(**A**) Spikes were identified by their prominence in the raw ORN recording. The inter-spike interval (ISI) was defined as the time from one spike to the next. A train with ≥2 spikes with ISI ≤ 50 ms was considered a burst. The intra-burst interval was the ISIs within a burst, the inter-burst interval (IBI) the ISIs between two bursts, omitting any individual spikes in between. The inter-event interval (IEI) included the ISIs between bursts and individual spikes. Detaching and reattaching the recording electrode to a long trichoid sensillum (**Bi**; paired t-test $t(9) = -2.184$; $p = 0.057$; $N = 10$) or adding DMSO to the SLR (**Bii**; Wilcoxon signed-rank test $Z = 0.153$; $p = 0.922$; $N = 10$) did not affect the mean spiking frequency.

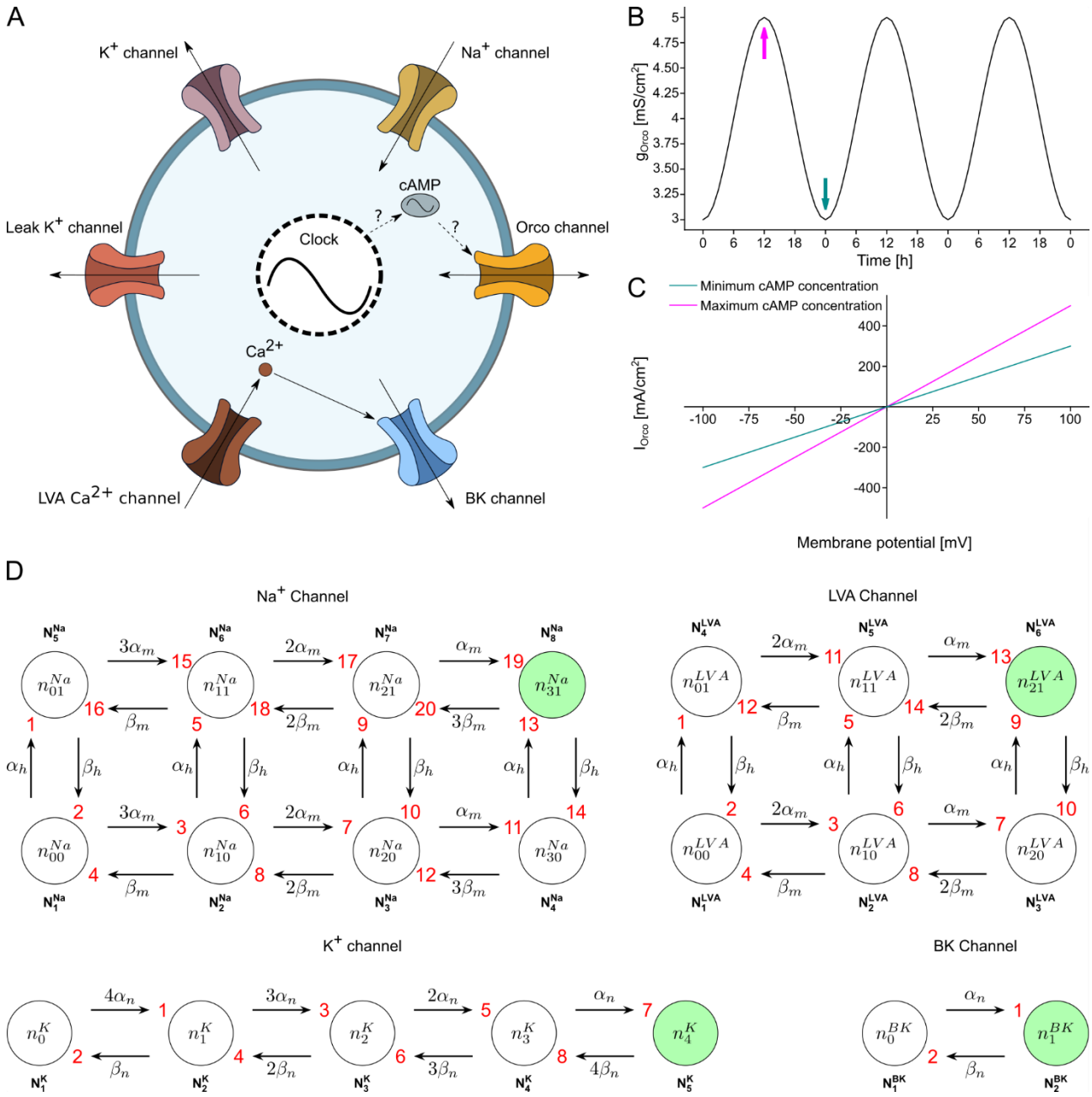

Figure 2: The conductance-based model of a simplified hawkmoth ORN.

(A) Schematic of the model containing a voltage gated sodium channel (Na^+), a voltage gated potassium channel (K^+), a low voltage activated calcium channel (LVA), a calcium and voltage activated potassium channel (BK), a leak channel, and a cAMP-gated leaky non-specific cation channel (Orco). The Orco channel is represented as a linear conductance whose value oscillates with a sinusoidal shape as a function of the ZT. The circadian rhythm in the Orco conductance is hypothesized to result from a cAMP-dependent increase in channel open-time probability (as found in *Drosophila* Orco: (Getahun et al., 2013)) via a circadian oscillation of antennal cAMP concentrations (Schendzielorz et al., 2015). This oscillation is driven by the circadian clock and serves as an input; the internal mechanism of the clock is not modeled explicitly. Arrows indicate the flow of ions through the channels. **(B)** Parametrized circadian oscillation in Orco conductivity,

introduced as an external input to our model, representing the gating of Orco by cAMP whose concentration oscillates on a circadian timescale. The times of minimum and maximum cAMP concentration are indicated by colored arrows. **(C)** Parametrized IV curve of the Orco channel showing a linear behavior with the slope depending on the cAMP concentration. Line colors correspond to the arrows in **B**. **(D)** Markov-chain representing all possible states and transitions for each type of ion channel included in the model. The per capita transition rates (α and β) depend on membrane potential and in the case of the BK channel also on the intracellular Ca^{2+}-concentration. The "N" state vectors contain the population of channels in each state "n". Directed edges are numbered in red. The only conducting state of each ion channel, representing the condition where all its gates are open, is shown in green.

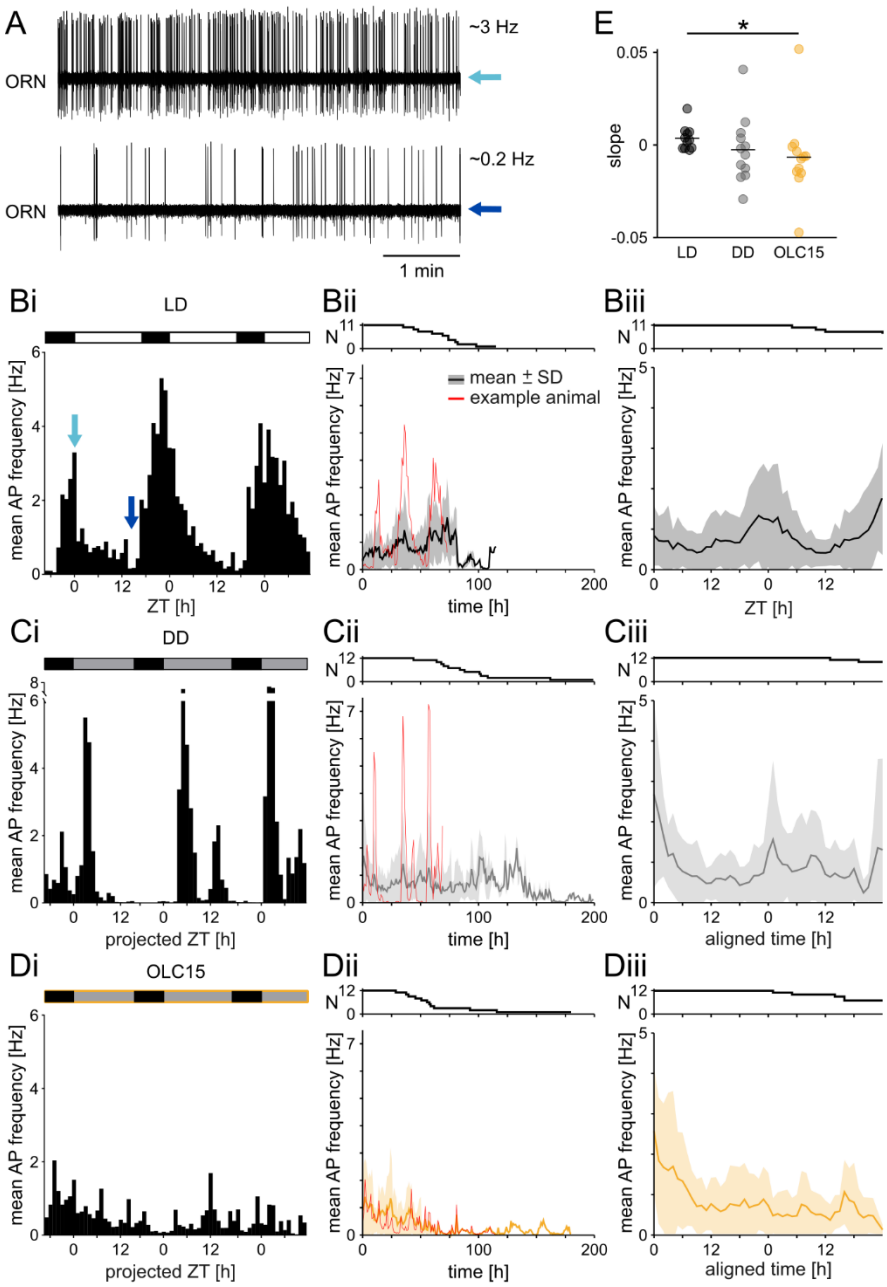

Figure 3: Spontaneous activity of pheromone-sensitive olfactory receptor neurons (ORNs) of male *M. sexta* shows Orco-dependent circadian modulation.

(A) Example tip recordings of the spontaneous activity of one long trichoid sensillum during a period of high (top, average frequency ~ 3 Hz) and low (bottom, average frequency ~ 0.2 Hz) activity. **(Bi)** Spontaneous spike frequency of one long-term ORN recording during 17:7 light-dark cycles (same experiment as in **A,** colored arrows indicate respective zeitgeber times (ZT)), indicated by the black-white bar at the top, increased during each activity phase and was low during the resting phases. Spike frequencies were averaged for each 1 h bin. **(Bii)** Mean spontaneous ORN spike frequency across all LD animals in 1 h bins. Data from the individual in **Bi** is highlighted in red. Recordings had different lengths, therefore the number of recordings used for the element-wise mean for each 1 h bin decreased with the time since the start of the recording, indicated in the top

panel. **(Biii)** Mean spontaneous ORN spike frequency across all LD animals in 1 h bins during the first 48 hours revealed circadian activity. **(Ci)** The spontaneous spike frequency of one long-term ORN recording in constant darkness (DD, the expected times of lights on are represented by grey bars above) exhibited a circadian pattern. The peak activity shifted in DD due to the animal's endogenous, free-running circadian period $\tau = 21.27$ h. **(Cii)** Mean spontaneous ORN spike frequency across all DD animals in 1 h bins. Data from the individual in Ci is highlighted in red. **(Ciii)** Mean spontaneous ORN spike frequency across all DD animals in 1 h bins during the first 48 hours after aligning the time to the first maximum in spontaneous activity (see Methods) revealed circadian activity. **(Di)** The spontaneous spike frequency of one long-term ORN recording in constant darkness with infusion of the Orco antagonist OLC15 (orange frame) dissipated the circadian rhythm of spontaneous activity. **(Dii)** Mean spontaneous ORN spike frequency across all OLC15 animals in 1 h bins. Data from the individual in **Di** is highlighted in red. In contrast to LD and DD conditions, the spike frequency decreases over time with prolonged exposure to OLC15. **(Diii)** Mean spontaneous ORN spike frequency across all OLC15 animals in 1 h bins (mean ± SD) during the first 48 hours after aligning the time to the first maximum in spontaneous activity (see Methods). In contrast to LD and DD conditions, the circadian change in spontaneous spiking frequency disappeared. **(E)** The slopes of the linear fits to the binned spiking activity of each individual animal in the three different conditions (see Methods). Each dot indicates the slope for one experiment. The line indicates the mean. The slope for OLC15 is significantly different from control LD.

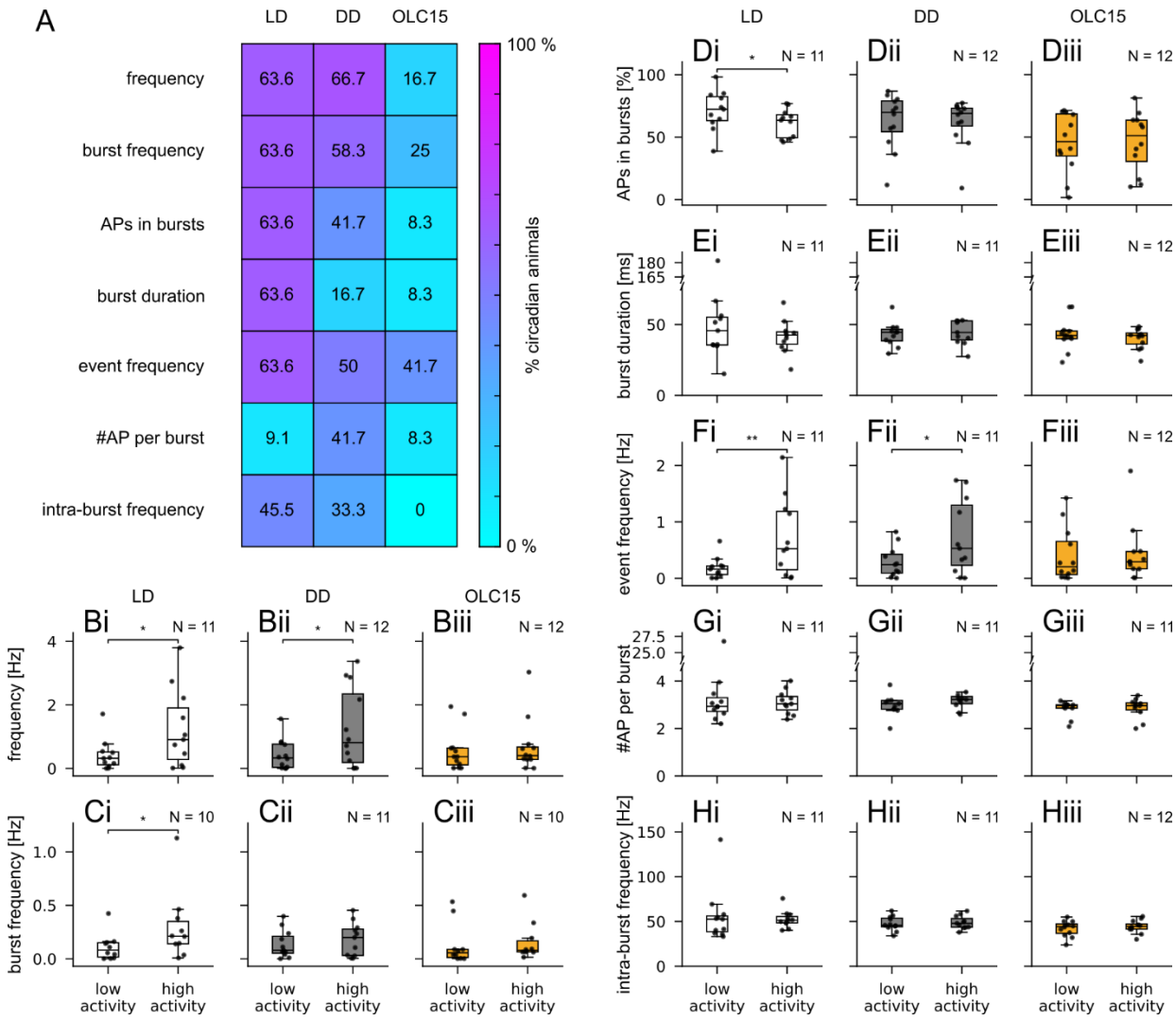

Figure 4: Blocking Orco removed circadian modulation of spontaneous ORN spiking patterns. RAIN analyses demonstrated significant circadian rhythmicity for most animals in most attributes of the spontaneous spiking activity in LD and DD conditions but not in OLC15 (**A**). Values and background colors indicate the percentage of animals that expressed significant circadian rhythmicity. Circadian differences of attributes were further quantified between the time windows of low vs. high activity (Wilcoxon signed-rank test, α = 0.05; **B-H**). Significant differences occurred mostly in LD (white boxes) and DD (gray boxes) conditions, but never when Orco was blocked with OLC15 (orange boxes). In both LD and DD, the mean spiking frequency was increased during high activity (**Bi, Bii**)**.** Only in LD but not in DD, the mean burst frequency (**Ci, Cii**) increased, whereas the relative number of spikes belonging to a burst (**Di, Dii**) decreased significantly during the high activity period. Both in LD and DD the mean event frequency (**Fi,Fii**) increased significantly. Mean burst duration (**Ei, Eii**), mean number of spikes per bust (**Gi,Gii**), and mean intra-burst intervals (**Hi, Hii**) did not differ between low vs. high spiking activity in LD and DD. When blocking Orco, the attributes for low vs. high activity did not differ for any of the attributes tested (**Biii-Hiii**). In DD and OLC15conditions, activity phases were aligned as described in the Methods; thus, low activity in

DD was at subjective ZT 19 and in OLC15 at subjective ZT 13, high activity was in both cases at subjective ZT 24. ZTs for low and high activity in LD were 10 and 0, respectively.

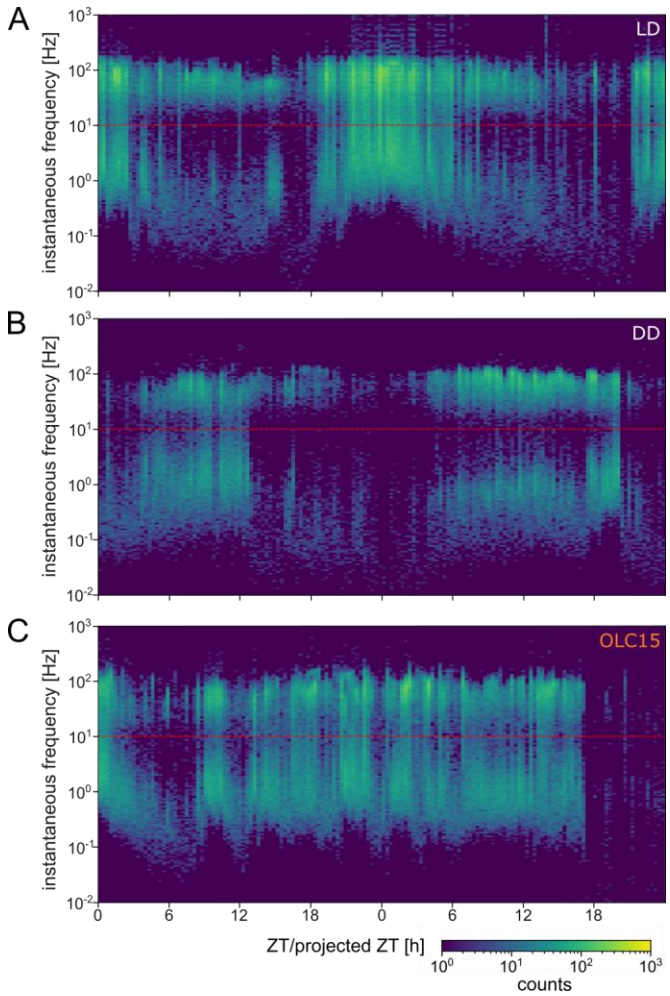

Figure 5: Blocking Orco removed circadian regulation of ultradian rhythms in the spontaneous ORN spiking pattern.

Heat map of the instantaneous frequencies (1/ISI) over two consecutive days of long-term tip recordings of one pheromone-sensitive long trichoid sensillum under different conditions (LD **(A)**, DD **(B)**, OLC15 **(C)**) in each panel. Representative recordings from one animal in each panel. Pixel color indicates the counts of instantaneous frequencies in that respective bin. The points fall mostly in a band of high frequencies (>10 – ~100 Hz) and low frequencies (0.01 – ~10 Hz), with the high-frequency band representing the instantaneous frequencies of spikes within a burst and the low-frequency band the instantaneous frequency between bursts. **(A, B)** The high frequency band indicates daily and circadian modulation of frequency prevalence. In addition, the low frequency band (<0.01 Hz to ~ 10 Hz) also displayed circadian modulation of the frequency composition. **(C)** Infusion of OLC15 deleted the circadian modulation in both frequency bands but not the ultradian rhythm of frequency prevalence.

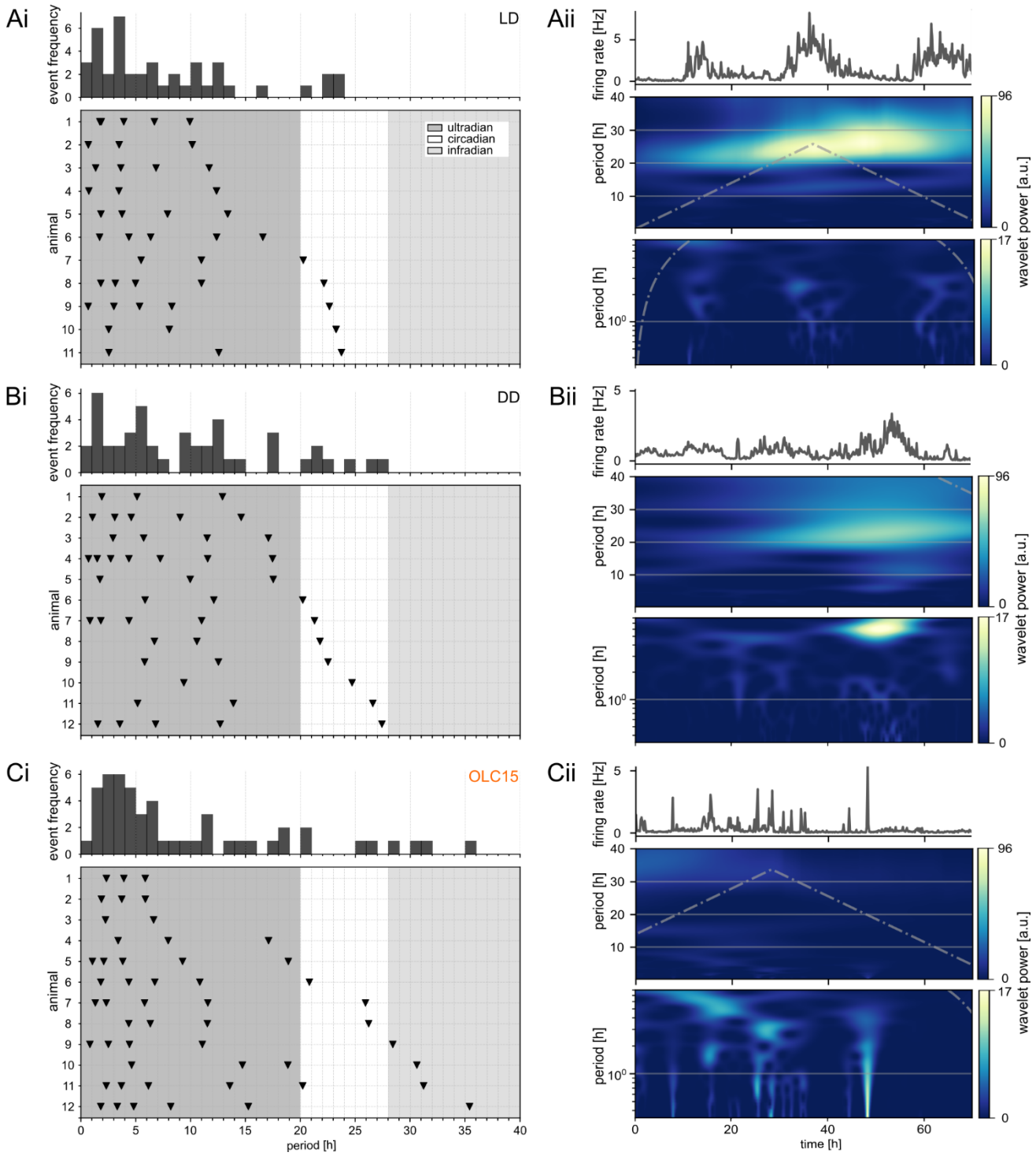

Figure 6: Blocking Orco affected ultradian and infradian frequencies in the spontaneous ORN firing patterns.

The Fourier analysis of spontaneous spiking activity revealed rhythms with ultradian (<20 h; dark grey), circadian (20-28 h; white), and infradian periods (>28 h; light grey) in LD (**Ai**), DD (**Bi**), and OLC15 (**Ci**). Each line represents one animal where each triangular marker is at the local maximum in the frequency spectra obtained for that animal. The histograms above illustrate how often

specific periods of spiking activity rhythms occurred averaged over all animals. Circadian rhythms were detected in LD (N = 5 of 11), DD (N = 7 of 10), and OLC15 (N = 4 of 12). Wavelet analysis of LD (**Aii**), DD (**Bii**), and OLC15 (**Cii**) confirmed the occurrence of multiscale periods. Example plots for one animal each, the same animals as in Figure 5. For each panel, the top plot depicts the mean firing frequency, the middle plot the wavelet power in the same period range as panels **i**, and the bottom plot the wavelet power for infradian periods up to 7 h on a log scale to highlight infradian time scales. Gray dashed lines indicate cone of uncertainty.

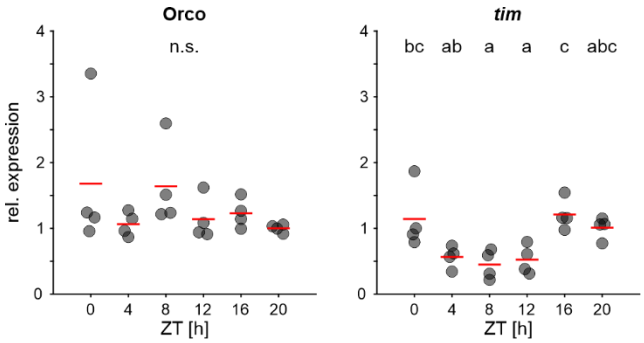

Figure 7: Orco is not under control of the TTFL-based molecular circadian clock.

Relative expression levels of *Orco* and *tim* mRNA from male hawkmoth antennae raised under LD conditions. *Orco* expression levels did not differ significantly between ZTs (ANOVA on ranks, $H(5) = 6.91$, $p = 0.227$: N = 4 per ZT). *tim* expression levels changed significantly throughout the day (1-way ANOVA, $F(5, 18) = 6.215$, $p = 0.002$) Red lines indicate mean, *tim* served as positive control.

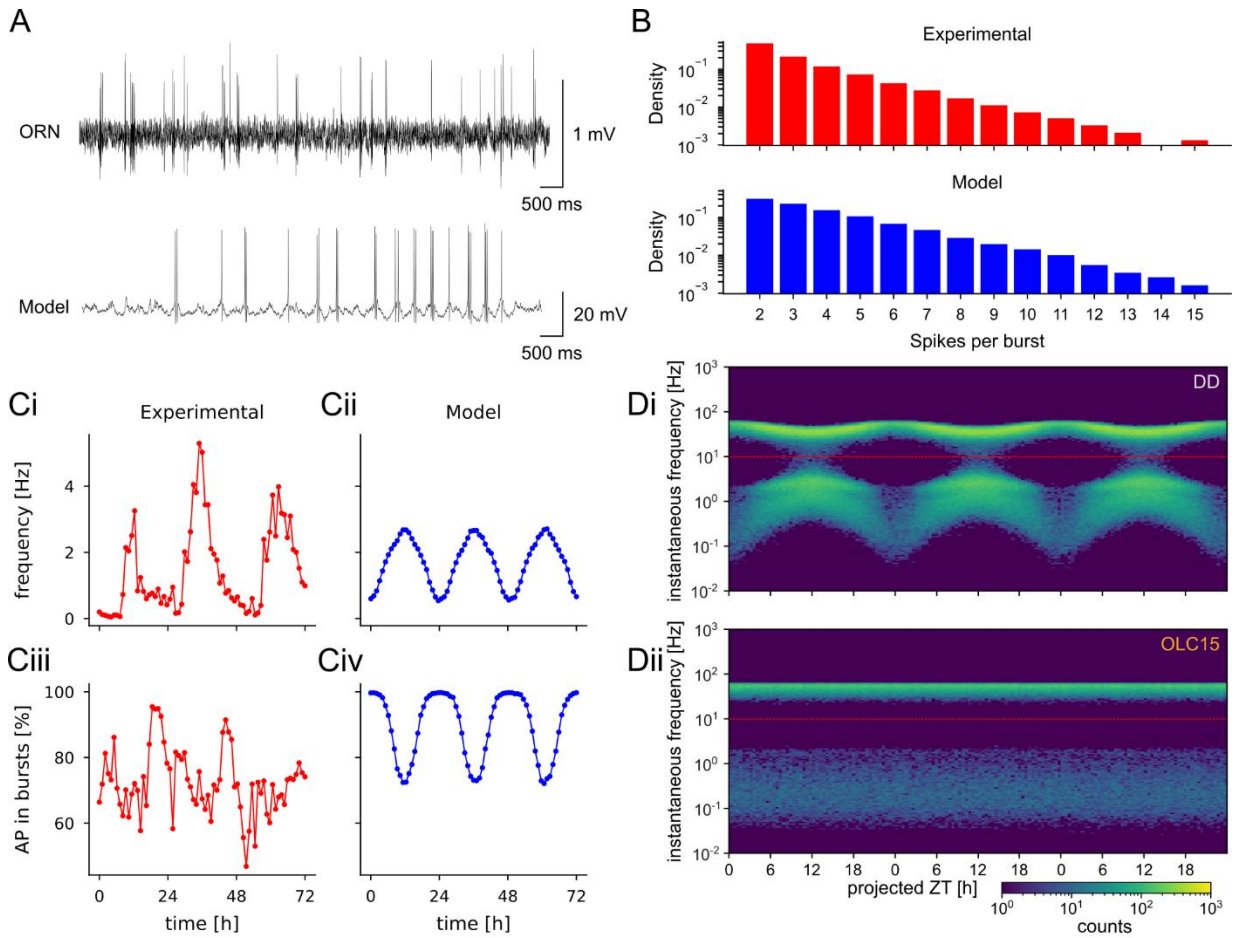

Figure 8: The model adequately reproduces the firing pattern of the biological ORN.

(A) The model activity (bottom trace) displays both isolated spikes and bursts of variable length as in the original recording (top trace). The model represents an intracellular recording whereas the biological recordings were done with extracellular electrodes. **(B)** Semi-logarithmic plot of burst length distribution of an experimental LD recording (top) and simulated model (bottom) of spontaneous action potential activity of pheromone-sensitive neurons. Both the model and the recordings display exponential decrease of the count's density as a function of the burst length, shown as a linear decrease in the logarithmic scale. **(C)** Comparison of the circadian modulationof model and ORN spiking attributes. Top panels (**Ci, Cii**) show mean spike frequency, whereas bottom panels (**Ciii, Civ**) show the percentage of spikes belonging to bursts. The simulated model reproduced the circadian dynamics observed in the experimental recordings, demonstrating good agreement between model and biological data. **(D)** Heat map of the simulated model, pixel color indicates the density of instantaneous frequencies in that respective bin. The points can be roughly divided in a band of high frequencies (top, ~50 – 80 Hz) and low frequencies (bottom, ~0.1 – 5 Hz), with the high-frequency band representing the instantaneous frequencies of spikes within a burst and the low-frequency band the instantaneous frequency between bursts. **(Di)** Simulated spikes with circadian regulation by the Orco channel; the inter-burst frequencies varied widely with circadian rhythmicity while the frequencies within burst remained approximately constant. The simulated results also reproduced the "merging" effect between the two bands when the bottom

one approaches the top one. **(Dii)** Simulated spikes without circadian regulation of Orco had no circadian oscillations.

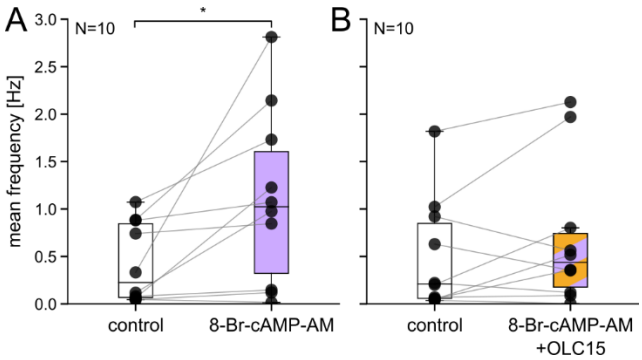

Figure 9: cAMP modulates open-time probability of Orco in M. sexta.

Perfusion of 8-Br-cAMP-AM significantly increased the spontaneous spiking activity at the end of the activity phase (ZT 1-3; **A**; Wilcoxon signed-rank test Z = -2.701; p = 0.004). However, activity did not increase when 8-Br-cAMP-AM was added together with the Orco blocker OLC15 (**B**; paired t-test t(9) = -1.446; p = 0.182). Electrodes were filled with SLR containing 0.1% and 0.15% DMSO as control in **A** and **B**, respectively. Data from individual animals are connected by lines.

9 Supplementary Material

9.1 Mathematical Model

The mathematical model is a 22-dimensional system of stochastic differential equations designed to describe the behavior of ion channels and their effects on the membrane potential. I_{LVA} represents a low-voltage-activated calcium current, while I_{Na} and I_K are the transient sodium and potassium currents responsible for action potential generation. I_{BK} is a large-conductance potassium channel that is activated by both a depolarized membrane potential and an increased intracellular calcium concentration, and I_L is the leak current. Additionally, the Orco channel is a leaky, non-specific ion channel gated by cAMP, with the cAMP concentration oscillating in a circadian rhythm. To model the Orco conductance, we used a sinusoidal function of Zeitgeber time (ZT), independent of the membrane potential, as shown in Figure 2B, C. Each of these ion channels has been reported in vitro in previous studies (Dolzer et al., 2021).

The deterministic part of the 22D model is given by the mean field of the channel-based Langevin model. This approach was introduced by Fox and Lu's (1994) for a 14D HH model. In their framework, one dimension tracks the membrane potential, while the other 13 dimensions correspond to the fraction of channels in each of the five states in the potassium (K^+) Markov chain and the eight states in the sodium (Na^+) Markov chain. Pu and Thomas (2020) demonstrated that the deterministic 14D model and the original 4D HH model are dynamically equivalent, meaning that each solution of the 4D model corresponds to a solution of the 14D model.

Expanding upon Pu and Tomas' methodology to represent out system, we added one dimension to track the calcium concentration, six dimensions for each possible state of the LVA channel, and two dimensions for each possible state of the BK channel. The state vectors for each ion channel are therefore defined as follows: a five-component vector NK for the K^+ gates, an eight-component vector NNa for the Na^+ gates, a six-component vector NLVA for the LVA gates, and a two-component vector NBK for the BK gates. The state vectors are represented as:

$$N^K = [n_{K0}, n_{K1}, n_{K2}, n_{K3}, n_{K4}]^T \in [0,1]^5 \quad (1)$$

$$N^{Na} = [n_{Na00}, n_{Na10}, n_{Na20}, n_{Na30}, n_{Na01}, n_{Na11}, n_{Na21}, n_{Na31}]^T \in [0,1]^8 \quad (2)$$

$$N^{LVA} = [n_{LVA00}, n_{LVA10}, n_{LVA20}, n_{LVA01}, n_{LVA11}, n_{LVA21}]^T \in [0,1]^6 \quad (3)$$

$$N^{BK} = [n_{BK0}, n_{BK1}]^T \in [0,1]^2 \quad (4)$$

The K^+ channel consists of four independent n (activation) gates, forming a five-vertex channel-state diagram with eight directed edges. The channel conducts a current only when it is in the rightmost state (Figure 2D). Similarly, the Na^+ channel is composed of three identical n gates and one h (inactivation) gate, forming an 8-vertex diagram with 20 directed edges, one of which is conducting. The LVA channel includes two identical n gates and one h gate, resulting in a 6-vertex diagram with 14 directed edges, one of which is conducting. The BK channel consists of a single n gate, forming a 2-vertex diagram with two directed edges, one of which is conducting. The Markov chain for every channel is shown in Figure 2B.

For a sufficiently large number of channels, Schmidt and Thomas (2014) and Schmidt et al. (2018) demonstrated that, under voltage clamp, the equations governing the system can be approximated by a multidimensional Ornstein-Uhlenbeck (OU) process, or Langevin equation, as follows:

$$dN^{ion} = \sum_{k=1}^{k_{max}} \zeta^{ion} \left\{ \alpha_k^{ion}(V) N_{i(k)}^{ion} dt + \sqrt{\epsilon^{ion} \alpha_k^{ion} \, N_{i(k)}^{ion} \, dW_k^{ion}} \right\} \tag{5}$$

Here ζ^{ion} is the stoichiometry vector for the kth directed edge. If we write i(k) for the source node and j(k) for the destination node of edge k, then $\zeta^{ion} = e_{j(k)}^{ion} - e_{i(k)}^{ion}$. The voltage-dependent per capita transition rate along the kth edge is $\alpha_k^{ion}(V)$ and $N_{i(k)}^{ion}$ is the fractional occupancy of the source node for the kth transition. The finite-time increment in the Poisson process is approximated by a gaussian process, namely, the increment dW_k^{ion} in a Wiener (Brownian motion) process associated with each directed edge. These independent noise terms are scaled by $\epsilon^{ion} = \frac{1}{N_{Tot}^{ion}}$, where $\frac{1}{N_{Tot}^{ion}}$ represents the total number of that specific ion channel.

The membrane potential is governed by the current balance equation:

$$C \frac{dV}{dt} = \sum_{\chi} I_{\chi} \tag{6}$$

where the set χ contains the six ionic currents included in the model:

$$\chi \in \{LVA, Na, K, BK, L, ORCO\} \tag{7}$$

Each of the six ionic currents included in the model are described as:

$$I_{Na} = -g_{Na} N_8^{Na} (V - V_{Na}) \quad (8)$$

$$I_K = -g_K N_5^K (V - V_K) \quad (9)$$

$$I_{LVA} = -g_{LVA} N_6^{LVA} (V - V_{LVA}) \quad (10)$$

$$I_{BK} = -g_{BK} N_2^{BK} (V - V_{BK}) \quad (11)$$

$$I_{Orco} = -g_{Orco} \left(0.8 + 0.2\, sin\left(\frac{2\pi t}{24h}\right)\right) (V - V_{Orco}) \quad (12)$$

$$I_L = -g_L (V_L - V) \quad (13)$$

Here, g_χ is the maximal conductance, V is the membrane potential, and V_χ is the reversal potential for each ion current. The parameter values for each current can be found in Table 1.

Each transition rate $\alpha_k^{ion}(V)$ is calculated in the following way:

$$\alpha_k^{ion}(V) = \frac{p_{j(k)\infty}^{ion}(V)}{\tau_p(V)} \quad (14)$$

where $p_{j(k)\infty}^{ion}(V)$ is the steady state value of the specific gate that switches states in the destination state and $\tau_p(V)$ is the time constant of said gate. The steady state activation values and time constants for the LVA, Na, K, and BK channels were based on Viertel and Borisyuk (2019). The steady state functions for the activation gates are denoted with m_∞^{ion}, and those for the inactivation gates with h_∞^{ion}.

Each gate's steady state activation function, except for the BK channel, takes the form:

$$p_{j\infty}^{ion}(V) = \frac{1.0}{1.0 + exp\left(\frac{(V - \theta_p)}{\beta_p}\right)} \quad (15)$$

The I_{BK} current is dependent on the intracellular calcium concentration and membrane potential as represented by the following equations:

$$m_{\infty}^{BK}(V) = \frac{1.0}{1.0 + exp\left(\frac{\left(V - V_{\frac{1}{2}}\right)}{(-15.6)}\right)} \tag{16}$$

$$V_{\frac{1}{2}} = -20 + 59.2e^{-90[Ca]} + 96.7e^{-470[Ca]} \tag{17}$$

$$\tau_{\alpha} = -(q - 1.0)\frac{(f - 0.2)}{0.8} + 170 \tag{18}$$

$$q = 2.9 + 6.3e^{-360[Ca]} \tag{19}$$

$$s = -25.3 + 107.5e^{-120[Ca]} \tag{20}$$

$$f = \frac{1.0}{10.0\left(e^{\frac{-(V+100.0-s)}{63.6}} + e^{\frac{(-150.0+(V+100.0-s))}{63.6}}\right)} \tag{21}$$

The intracellular concentration of calcium ions is described by the following equation:

$$\frac{d[Ca]}{dt} = -\gamma\frac{I_{LVA}}{zFd} + \frac{[Ca_0] - [Ca]}{\tau_{Ca}} \tag{22}$$

where Ca_0 is the steady state calcium concentration, γ describes calcium buffering, z is the ionic valence of calcium, F is Faraday's constant and d is the depth in microns at which calcium ions concentrate near the membrane.

The parameters of each steady state activation function as well as the time constant for each gating value can be found in Table 2.

Table 1: Parameter values for model currents.

Current	g_X (mS/cm^2)	V_X (mV)
I_L	4.3	-62.5
I_{LVA}	10.0	120
I_{NA}	29.17	45.0
I_K	12.96	-105.0
I_{BK}	9.0	-105.0
I_{ORCO}	5.0	0.0

Table 2: Gating variable parameter values.

Variable	θ	β	τ(ms)

m^{LVA}	-30	-4.8916	$\frac{40.0}{cosh\left(\frac{(V+37.1)}{9.7832}\right)}$
h^{LVA}	-59.2	11.2326	$\frac{350.0}{cosh\left(\frac{(V+59.2)}{22.4652}\right)}$
m^{Na}	-25.0	-6.5	0.2
h^{Na}	-26.0	9.0	$\frac{10.0}{cosh\left(\frac{(V+26.0)}{18.0}\right)}$
m^{K}	-26.0	-9.0	$\frac{10.0}{cosh\left(\frac{(V+26.0)}{18.0}\right)}$

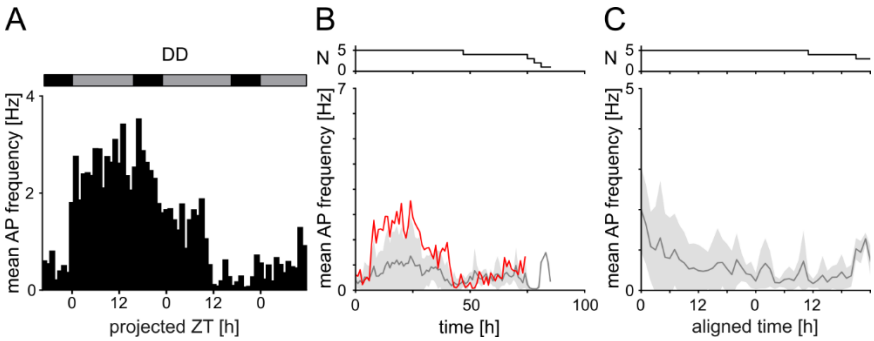

Figure 3 – Supplement: Spontaneous spiking activity of ORNs of pheromone-exposed male *M. sexta*.

To enhance synchronization, males were exposed to females and pheromones as additional zeitgeber for 30 mins at ZT 16 before the start of the experiment. Recordings were obtained over multiple days in DD. **(A)** The spontaneous spike frequency of one long-term ORN recording in constant darkness (DD, the expected times of lights on are represented by grey bars above) **(B)** Mean spontaneous ORN spike frequency across all DD animals in 1 h bins. Data from the individual in **A** is highlighted in red. **(C)** Mean spontaneous ORN spike frequency across all DD animals in 1 h bins during the first 48 hours after aligning the time to the first maximum in spontaneous activity (see Methods). No circadian activity was evident in these pheromone-exposed males.